Modeling of Ionization Phenomena in Premixed Laminar Flat Flames using FGM

Keelara Chandrashekar, Adithya

Award date:
2018

Technische Universiteit
Eindhoven
University of Technology

Eindhoven University of Technology

Modeling of Ionization Phenomena in Premixed Laminar Flat Flames using FGM

Master Thesis

Adithya Keelara Chandrashekar (0979634)

Supervisors:
dr.ir Jeroen van Oijen
dr.ir Nijso Beishuizen
Committee members:
dr.ir Rob Bastiaans
dr.ir Clemens Verhoosel

A thesis submitted in fulfillment of the requirements for the degree of Master of Science

in the

Multiphase and Reactive Flows Research Group
Department of Mechanical Engineering

in collaboration with

BOSCH
Invented for life

To my parents

Abstract

In this study, the ionization phenomenon is modeled using Flamelet Generated Manifold (FGM) method, to detect the electric current under the influence of an applied electric potential for flat methane-air flames. The FGM method is a reduction method used to solve chemically reactive flows. FGM method uses a manifold to look up the flame properties, by solving a small number of so-called control variables equations mainly progress variable and enthalpy.

The source terms of the charged species (H_3O^+, e^-) are not only a function of progress variable and enthalpy, but also a function of an applied electric field. This makes FGM method to solve an additional equations for charged species and potential. This approach yields a good validation between the FGM method and the detailed mechanism GRI-Mech 3.0 result, for all applied potential in one-dimensional domain. GRI 3.0 mechanism contains 325 reactions which includes 53 species, to model combustion.

The FGM method is then extended into two-dimensional domain to check the accuracy of the model. For non-saturation electric field, FGM method computes higher potential distribution in the domain which is caused due to the higher charge density. This leads to the saturation of the electric field at lower potential compared to detailed and experimental results. Considering the electrode to be adiabatic, the saturation electric current computed compares well with detailed chemistry results. However, the saturation electric current computed due to the cooling of the electrode compares well with the experimental results. Due to the heat loss effects, the production rate of charged species is lower than the adiabatic case, which results in a current higher than the detailed chemistry result by 10 μA.

Contents

List of Figures

Chapter 1

Introduction

1.1 Background

Fire is the common form of combustion, on which humans have been dependent on from an early stages of their life. It has been used from cooking to launching rockets to the space. Most of this combustion process is mainly from burning of fossil fuels. The main disadvantages of burning fossil fuels are; formation of green house and toxic gases, for example CO_2 and NO_x respectively.

Looking at the human history the use of combustion has changed over the years. It is known that ancient Greeks originally developed the central heating system, where the temple of Ephesus was heated by flues of a boiler. This was planted underground and heat was circulated by combustion. Nowadays, there are many types of central heating systems, such as wood fired, gas fired central systems etc. A wood fired central system produces more carbon products when compared to gas fired and hence, less environmental friendly. Initially gas fired central systems used diffusion flame, where fuel and oxygen were fed into gas chamber separately for combustion. This has been replaced by lean premixed methane-air flame, due to the production of low NO_x and CO emissions.

In order to burn lean combustion and to reduce NO_x and CO emissions, central heating systems have been integrated with smart control systems, which help to curb the emission. This is where the flame ionization comes into play, because the control circuits use the presence of charged species in flames, by the application of external electric field across the flame. This results in an electric current from which two important properties can be determined: 1) The fuel-air ratio (equivalence ratio), 2) Presence of a flame in the combustion chamber. If no electric current is detected, then it means that there is no flame in the combustion chamber. Moreover, an increase in current indicates increase in fuel-air ratio.

Controlling the current measured in a flame, the fuel-air ratio can be controlled. Lean combustion (fuel-air ration below 1) reduces production of CO. As CO is a colorless, odorless, tasteless gas, and is very toxic to haemoglobic animals, and NO_x contributes to the formation of smog and acid rain, which can be reduced by reducing the temperature in the combustion chamber.

Detection of an electric current implies the presence of charged molecules in the flame. The presence of ions and electrons can be detected in all carbon based flames [10], [12]. In a lean combustion most of the ions are produced from the main reaction involving CH and O. When an external electric field is applied, charged species experience an electric force, due to which,

electrons and ions moves towards positive and negatively charged electrodes respectively. This results in an electric current. Increasing the electric field increases the electric current. However, the current reaches a saturation level for certain applied potential. Furthermore, increasing the potential doesn't increase the current. This is due to complete charge separation of ions and electrons, which results in no recombination reaction after combustion [27].

Previous work by Speelman et al [27] was focused on modeling electric currents in flat flames, under the influence of an applied electric field in one-dimensional domain. They also investigated saturation of the electric current and the diodic effect of the methane-air flat flames. The model was implemented in CHEM1D [25], a flame simulation software which computes temperature and species in one-dimensional flows. The present study continues the work of Speelman and extend it to multi-dimensional flows using Flamelet Generated Manifold (FGM).

The new model uses the Flamelet Generated Manifold (FGM) [21] method, which solves control variables. All other values are looked-up according to the solutions of the control variables. This reduces the computational time without loosing too much accuracy of the results.

This thesis will focus on extending the one-dimensional model into a two-dimensional model using Ansys Fluent. Two-dimensional results are compared with one-dimensional results and simulated electric currents are validated against experimental data. This work focuses on flat methane-air flames, with varying applied electric field for different equivalence ratio. This chapter introduces the ionization mechanism in flames and the Flamelet Generated Manifold method. Finally the objectives of this study are discussed.

1.2 Ionization mechanism in flames

For the past few decades, research on ionization phenomenon of flames has recieved a lot of importance. As flames are considered to have small amount of charged species, this enables it to behave as a weakly ionized plasma. This research has given spark ignition research field to improve the ignition of fuel-air mixtures. Another important application of this is in combustion applications like, heating boilers. By applying strong electric field carbon flames can be stabilized [3] and fuel-air ratio can be controlled by the measured current.

The source of charged species is widely accepted to come from the so-called chemi-ionization reaction, which is given by [3]

$$\mathrm{CH} + \mathrm{O} \rightarrow \mathrm{CHO}^+ + \mathrm{e}^-. \tag{1.1}$$

In recent research [16], it has been found that in rich hydro-carbon flames there is an additional chemi-ionization reaction which is given by,

$$\mathrm{CH} + \mathrm{C_2H_2} \rightarrow \mathrm{C_3H_3^+} + \mathrm{e}^- \tag{1.2}$$

As this research does not focus on rich fuel-air mixtures, only reaction (1.1) is considered. CHO^+ reacts quickly with $\mathrm{H_2O}$ to form $\mathrm{H_3O}^+$, following reactions are given to be

$$\mathrm{CHO}^+ + \mathrm{H_2O} \rightarrow \mathrm{H_3O}^+ + \mathrm{CO}, \tag{1.3}$$

This reaction is called proton transfer reaction. Then it leads to recombination reaction which is written as

$$\mathrm{H_3O}^+ + \mathrm{e}^- \leftrightarrow \mathrm{H_2O} + \mathrm{H}. \tag{1.4}$$

Charged species from equations (1.1), (1.3) and (1.4) have been implemented in CHEM1D and compared its concentrations against the experimental results [27].

In the past few decades there has been quite some research on determining the charged species in flames for different equivalence ratios. Most of them are experimental research and very few numerical models exits. In most numerical models generally the electric current is not taken into account, when potential is applied across the flame. However, the model from Speelman which this study is based upon, has modeled one-dimensional flat methane-air flames in CHEM1D. This model can be used to simulate electric current for different equivalence ratios, when an external electric field is applied at a distance.

1.3 Objective of this study

The existing CHEM1D model computes temperature and neutral species distribution in one-dimensional chemically reacting flames. Apart from this, it also computes the distribution of charged species, under the influence of an applied electric field. The model also computes the electric current due to electric field, and has been compared with the experimental results [27].

The main objective of this study is to model the ionization mechanism using FGM method and to implement it in a two-dimensional model. As the FGM model does not solve all the species equations, it is important to simplify the diffusion model. For this, two simplified diffusion models are implemented for the ionization model, and compared with the multi-component diffusion model [27].

Before implementing the FGM model in a multi-dimensional solver, a validation of the FGM method against the 1D detailed model is performed. One of the important parameters which can be verified with experimental results is the electric current. Therefore, the electric current is verified at every stage, to check the accuracy of the FGM model.

Finally, the FGM model is implemented in a two-dimensional geometry. Considering the electrode to be adiabatic and cold, the ionization mechanism is compared with the detailed results. The model is also used to study the diodic effect. To conclude, the current is determined from each case and compared with both experimental results and with detailed chemistry results.

1.4 Thesis outline

First in the next chapter, the theoretical framework is presented for combustion of fluid flows. This includes the effect of electric field for the charged species. Further different transport model are discussed for the simplification of diffusion. Chapter 2, also discusses the modeling of ionization model for FGM method using constant Lewis diffusion model. It is concluded with the FGM implementation using the CFD code for multi-dimensional method.

In Chapter 3, different diffusion models are compared and a simple diffusion model is considered for further computation to reduce the computational time. Further, the model is used to study the effect of charged species, on applied potential for parameter like equivalence ratio and electrode distance. Finally, the FGM model is validated against the detailed chemistry model and the simulated electric current is compared.

With the implementation of the FGM method in CFD software package Fluent, Chapter 4 discusses the two-dimensional model description of the heat flux burner. Then the results are presented for various electric field condition saturation and non-saturation conditions. To check the accuracy of the FGM method, the two-dimensional model results are compared with the detailed chemistry results. The model is also used to verify the diodic effect and heat loss effects at the electrode. This will be followed by conclusion and recommendation in Chapter 5.

Chapter 2

Theoretical framework

In this chapter the model developed to predict the electric current in flat methane-air flames in the presence of an applied external electric field, will be discussed. Required relations to build the model are then explained, this includes fluid flow relations and electric field relations. This chapter also describes the implementation of Flamelet Generated Manifold, for ionization model and also explains the manifold taken for the computation of flat methane-air flames.

2.1 Governing equations

This section focuses on the conservation equations which are needed to model the flow problem encountered in this study. This includes conservation of mass, momentum and energy equations. Then a species conservation equation is added, to describe the solution of species in the chemically reacting flows. Thermodynamic relation are used to close the set of equations to determine the flow problem. After that transport chemistry is discussed which include multi-component, constant Lewis and mixture average diffusion models.

2.1.1 Conservation equations

As mass is neither created nor destroyed, conservation of mass is given by [1]

$$\frac{\partial \rho}{\partial t} + \nabla \cdot (\rho \mathbf{v}) = 0, \tag{2.1}$$

where ρ, t, and $\mathbf{v}$ represent density, time, and velocity vector respectively.

The conservation of momentum is given by [1]

$$\frac{\partial \rho \mathbf{v}}{\partial t} + \nabla \cdot (\rho \mathbf{v}\mathbf{v}) = -\nabla p - \nabla \cdot \bar{\bar{\tau}} + \rho \mathbf{g} + \mathbf{F}_e, \tag{2.2}$$

$$\mathbf{F}_e = q\mathbf{E} \tag{2.3}$$

where $\bar{\bar{\tau}}$ is Newtonian stress tensor, p is pressure, $\mathbf{g}$ is the gravitational force, $\mathbf{F}_e$ is the electric force density of the external field and it is neglected, q is the charge density and $\mathbf{E}$ is the electric

field strength. The conservation of energy is most commonly expressed in terms of enthalpy in combustion. This enthalpy conservation is given by [26]

$$\frac{\partial \rho h}{\partial t} + \nabla \cdot (\rho h \mathbf{v}) = \mathbf{v} \cdot \nabla p + \frac{\partial p}{\partial t} - \nabla \cdot \mathbf{q} + (\bar{\bar{\tau}} \cdot \nabla) \cdot \mathbf{v} + \mathrm{W}_e, \tag{2.4}$$

$$\mathrm{W}_e = \sum_{i=1}^{N_s} q_i \mathbf{E} \cdot (\mathbf{v} + \mathbf{V}_i), \tag{2.5}$$

where $\mathbf{q}$ is the heat flux and W_e is the work done on the flow by the external force $\mathbf{F}_e$. Viscous stress tensor for Newtonian fluid is given by

$$\bar{\bar{\tau}} = -\mu \left[\nabla \mathbf{v} + (\nabla \mathbf{v})^T - \frac{2}{3} (\nabla \cdot \mathbf{v}) \mathrm{I} \right], \tag{2.6}$$

where μ is the dynamic viscosity of the gas mixture calculated as [31]

$$\mu = c_p \cdot 1.67 \times 10^{-8} \left(\frac{T}{T^o} \right)^{0.51}. \tag{2.7}$$

As the equation is solved as steady sate and the work done is considered to be zero, the enthalpy conservation equation (2.4) can be written as,

$$\frac{\partial \rho h}{\partial t} + \nabla \cdot (\rho h \mathbf{v}) = -\nabla \cdot \mathbf{q}.$$

To describe the distribution of chemical species in combusting flow, the conservation of species is written as

$$\frac{\partial \rho Y_i}{\partial t} + \nabla \cdot (\mathbf{v} + \mathbf{v}_i) = \dot{\omega}_i, \qquad i = 1, ..., N_{\mathrm{sp}}, \tag{2.8}$$

where Y_i, $\dot{\omega}_i$ and v_i represents mass fraction, source term and diffusion velocity of species i respectively. Since sum of mass fraction of all the species $(\sum_{i=1}^{N_{sp}} Y_i) = 1$, substituting 2.8 in 2.1 gives,

$$\sum_{i=1}^{N_{sp}} \dot{\omega}_i = 0. \tag{2.9}$$

This suggests that sum of all the species source term is zero in steady state.

2.1.2 Thermodynamic equations

In this section thermodynamic variables are derived to close the equation which are explained in section (2.1.1). The variables ρ, $\bar{\bar{\tau}}$ and h are defined by well known thermodynamic relations.

Since this study involves low pressure and high temperature, the ideal gas law can be used to derive the density ρ. The ideal gas law relation is given by

$$p = nRT, \tag{2.10}$$

where n, T, and R represents molar density, temperature and universal gas constant respectively. Molar density is related to mass density ρ by

$$n = \frac{\rho}{\bar{M}}, \tag{2.11}$$

where $\bar{M}$ is the mean molar mass of the mixture.

The caloric ideal gas law is used to relate temperature (T) and specific enthalpy (h) for species i. This is given by

$$h_i = h_i^o + \int_{T^o}^{T} c_{p,i}(\xi) d\xi, \tag{2.12}$$

where h^o is the enthalpy at a standard state and c_p is the specific heat capacity at a constant pressure. Now total enthalpy is defined as

$$h = \sum_{i=1}^{N_{sp}} Y_i h_i, \tag{2.13}$$

and total specific heat capacity is defined as

$$c_p = \sum_{i=1}^{N_{sp}} Y_i c_{p,i}. \tag{2.14}$$

2.1.3 Transport chemistry model

One of the topic in this study is to compare different diffusion models and how they effect the diffusion of charged species on an applied potential. Three different diffusion models are considered, with multi-component being the most detailed and constant Lewis being the least detailed diffusion model. The multi-component model has already been modeled and implemented for ionization mechanism. In this study mixture-averaged and constant Lewis diffusion model, are modeled for ionization phenomenon and compared with multi-component diffusion model.

Multi-component diffusion model

This is the most detailed model for computing diffusion of species, this has been studied and implemented [27] with the inclusion of ionization mechanism. So, this section briefly discuss about the implementation.

Diffusion flux, $\rho Y_i \mathrm{v}_i$, for the multi-component diffusion model is given as

$$\rho Y_i \mathrm{v}_i = -D_i^T \nabla \ \ln \ T - \rho Y_i \sum_{j=1}^{N_{sp}} D_{ij} d_j, \qquad i = 1, ..., N_{sp}, \tag{2.15}$$

where D_{ij} and D_i^T are generalized diffusion coefficients and thermal diffusion coefficients respectively, these are found by solving transport linear systems and dependent on the concentration of species in the mixture [27]. The diffusion vector d_j is represented by

$$d_j = \nabla X_j + X_j \left(1 - \frac{M_j}{\bar{M}}\right) \nabla \ \ln \ p - \frac{\rho}{p} \left(Y_j b_j - Y_j \sum_{k=1}^{N_{sp}} Y_k \mathbf{b}_k \right), \quad j = 1, ..., N_{sp}, \tag{2.16}$$

where X_j and M_j represents mole fraction and molar mass respectively of species j and b_j represents the acceleration caused by external forces acting upon species j, which is electric field in this case written as

$$b_j = \frac{N_A}{M_j} \mathbf{f}_{e,j}, \tag{2.17}$$

where $\mathbf{f}_{e,j}$ is the body forces on species j.

Mixture-averaged diffusion model

In the mixture-averaged, the diffusion velocity of each gas is calculated by approximating all the other gases velocity as equal. So, only one diffusion term, D_i is calculated for each species. Diffusion velocity is written as

$$v_i = -\frac{1}{X_i} D_i d_i - \frac{D_i^T}{\rho Y_i} \nabla \ln\ T, \tag{2.18}$$

mixture diffusion coefficient for species i is written as

$$D_i = \frac{\sum_{j \neq i} X_j W_j}{\bar{W} \sum_{j \neq i} X_j \mathcal{D}_i} = \frac{1 - Y_i}{\sum_{j \neq i} X_j / \mathcal{D}_i}, \tag{2.19}$$

where $\mathcal{D}_i$ is the binary diffusion coefficient, which is diffusivity of species i. Through Einstein relation it can be written that

$$\mu_i = q_i \frac{\mathcal{D}_i}{k_b T} \tag{2.20}$$

where μ_i is the binary mobility and k_b is the Boltzmann's constant.

Since the mass fraction of charged species is usually small in the flame, the approximation 1-Y_i is used. Now, the diffusion velocity is simplified as,

$$v_i = -D_i \frac{\nabla X_i}{X_i} + S_i \mu_i E, \tag{2.21}$$

where $S_i = q_i/|q_i|$ is the charge sign of the charged species i.

Constant Lewis diffusion model

Above two diffusion model explained are both computationally intensive. In order to make it simplified, a Fick-like diffusion model is used. Here dimensionless Lewis number Le, is used to calculate diffusion coefficient, which is the ratio of thermal conduction to species diffusion given by

$$Le_i = \frac{\lambda}{\rho D_i c_{p_i}}, \tag{2.22}$$

where λ is the thermal conductivity. From Eq 2.22 the species diffusion fluxes can be expressed as

$$\rho v_i Y_i = -\frac{\lambda}{Le_i c_{p_i}} \nabla Y_i, \tag{2.23}$$

where Lewis number (Le) is assumed constant.

2.2 Maxwell's and closure relations

In the previous section fluid flow relations are described by using Navier-Stokes equations. These equations also take external forces into account. In order to compute these external forces electric and magnetic fields must be known. When these forces are determined electric force density, F_e,

and the work done by the electric field on the flow, W_e, can be computed. These two can then be substituted in equations (2.2) and (2.4) respectively.

First Maxwell's equations are used to compute the electric field with closure equations. Then these closure relations are used to couple the electric field to the fluid flow field.

Maxwell's relations

The electric field, **E**, and the magnetic field, **B**, are related using the Maxwell-Faraday equation, which is given by

$$\nabla \times \mathbf{E} = -\frac{\partial \mathbf{B}}{\partial t}. \tag{2.24}$$

Differential equation of the Ampere's circuit law with the addition of the Maxwell equation couples electric and magnetic fields with the current density **J**, in the form

$$\nabla \times \mathbf{B} = \mu_0 \mathbf{J} + \mu_0 \varepsilon_0 \frac{\partial \mathbf{E}}{\partial t}, \tag{2.25}$$

Where μ_0 and ϵ_0 are the permeability and permittivity of free space. To couple electric field to the charge density, q, the third Maxwell relation is used which is the Gauss's law, given by

$$\nabla \cdot \mathbf{E} = \frac{q}{\varepsilon_0}. \tag{2.26}$$

By using the Gauss's law for magnetism which is the last Maxwell's relation, we know the magnetic flux density is zero everywhere and is denoted by

$$\nabla \cdot \mathbf{B} = 0. \tag{2.27}$$

By taking the divergence of equation (2.25) and substituting in (2.26), charge continuity equation can be obtained as

$$\frac{\partial q}{\partial t} + \nabla \cdot \mathbf{J} = 0. \tag{2.28}$$

Assuming magnetic field are not time-varying, written as

$$\frac{\partial B}{\partial t} = 0, \tag{2.29}$$

then by Faraday's law the electric field is curl free. In this case, the electric field can be written as the gradient of a scalar potential and is given by

$$\nabla \phi = -\mathbf{E}, \tag{2.30}$$

where ϕ is the electric potential. Substituting equation (2.26) in (2.30) leads

$$\nabla^2 \phi = -\frac{q}{\varepsilon_0}. \tag{2.31}$$

This is the Poisson's equation which will be used to solve potential equation.

Closure relations

Now in order to couple the Maxwell's equations to the Navier-Stokes equation, charge density, q, should be formulated. The charge density is a function of the molar density of the charged particles and their charge, given by

$$q = \sum_{i=1}^{N_{sp}} q_i = eN_A\rho \sum_{i=1}^{N_{sp}} S_i \frac{Y_i}{M_i}, \tag{2.32}$$

where e is the elementary charge, N_A is Avogrado's number and S_i is the species charge number.

One way to verify the implementation of ionization mechanism is correct is by calculating the electric current (I). Electric current can be calculated by

$$I = \int\int_S \mathbf{J} \cdot \mathbf{n} dS, \tag{2.33}$$

where $\mathbf{n}$ is the local domain outward unit vector and the current density, $\mathbf{J}$, is defined as

$$\mathbf{J} = \sum_{i=1}^{N_{sp}} q_i(\mathrm{v} + \mathrm{V}_i). \tag{2.34}$$

2.3 Combustion chemistry equations

In this section equations needed to describe the combustion chemistry are given. This involves the calculation of the source term, $\dot{\omega}_i$, which are given by species conservation Eq 2.8. This study involves complex reactions of hydrocarbons. For this GRI3.0 mechanism [24] is considered with the implementation of ionization mechanism [27]. This mechanism involves 53 neutral species with the addition of 3 charged species and 328 reactions in total.

The forward and reverse reactions are described by

$$\sum_{i=1}^{N_{sp}} \nu_i' M_i \leftrightarrow \sum_{i=1}^{N_{sp}} \nu_i'' M_i, \tag{2.35}$$

where M_i represents a species in the model and the difference $\nu_i'' - \nu_i'$ is the stoichiometric coefficient of the reaction k. The reaction rate, r_k for any reaction is given by

$$r_k = k_f \prod_{i=1}^{N_{sp}} \left[M_i^{\nu_i'}\right] - k_r \prod_{i=1}^{N_{sp}} \left[M_i^{\nu_i''}\right] \tag{2.36}$$

where f and r represents the forward and reverse of reaction. The reaction rate coefficient k, can be computed by using the Arrhenius equation

$$k = AT^{\beta} \exp\left(-\frac{E_a}{RT}\right), \tag{2.37}$$

where A and β are the constants, and E_a is the activation energy of the reaction.

The species source term, $\dot{\omega}_i$, is finally given by

$$\dot{\omega}_i = M_i \sum_{k=1}^{N_r} \nu_i r_k, \tag{2.38}$$

where N_r is the number of reactions. Now equation (2.38) is substituted into equation (2.8) for calculating species balance.

2.4 Flamelet Generated Manifold

In a detailed chemistry simulation, all N_{sp} species equations are solved 2.8. This means that for each species i a differential equation is solved including mass, momentum, and energy equations. As the mechanism GRI3.0 used in this study consists of 56 species, solving all equations for a two dimentional domain will be very CPU intensive. In order to simplify this, the Flamelet Generated Manifold (FGM) is used. In the FGM method the flame is represented by a scalar called progress variable $\mathcal{Y}$. This progress variable should either increase along the flamelet or decrease.

A multi-dimensional flame is considered, as a set of one-dimensional flames in FGM. In advance these one-dimensional flat flames are solved and stored in a database. The thermochemical composition terms Y_i, T is saved as a function of the progress variable. Now, this way only one differential equation is solved for progress variable, together with mass, momentum and enthalpy equations. The progress variable considered in this study will be CO_2. Progress variable zero mass fraction represents unburnt mixture and maximum mass fraction in the flamelet represents burnt mixture. The database must contain a full range of CO_2 mass fraction for computing combusting flow problems.

2.4.1 Flamelet equations

A flamelet is an adiabatic one-dimensional flat flame structure [21]. In order to compute these flamelets a flame code CHEM1D [25] is used, which solves quasi-one-dimensional equations to generate these flamelets. Steady one-dimensional mass, energy and species conservations flamelet equations are given by

$$\frac{\partial m}{\partial s} = 0, \tag{2.39}$$

energy equation for constant Lewis model is written as

$$\frac{\partial (mh)}{\partial s} - \frac{\partial}{\partial s}\left(\frac{\lambda}{c_p}\frac{\partial h}{\partial s}\right) = \frac{\partial}{\partial s}\left(\frac{\lambda}{c_p}\sum_{i=1}^{N_s}\left(\frac{1}{Le_i} - 1\right)\frac{\partial Y_i}{\partial s}\right), \tag{2.40}$$

Species equation is written as

$$\frac{\partial (mY_i)}{\partial s} - \frac{\partial}{\partial s}\left(\frac{\lambda}{Le_i c_p}\frac{\partial Y_i}{\partial s}\right) = \dot{\omega}_i, \qquad i = 1, ..., N_s, \tag{2.41}$$

where m is mass burning rate and s is the flame surface.

The solution of these set of 1D equations (2.39)-(2.41), are called flamelets. For the enthalpy equation (2.40), the R.H.S is neglected. This makes the solution simpler as the gradient of the species are not solved. This does not change the solution of the enthalpy, instead it makes the solution much simpler to compute giving a constant solution.

2.4.2 Manifold construction

In order to create a manifold first a flamelet is calculated, which is done by solving equations (2.39)-(2.41). Now these flamelets are stored in a database, which is stored in such a way, that it is easy for a CFD code to read the manifold and retrieve values. To include enthalpy changes, first adiabatic flamelets are solved for various unburnt temperatures (T_u). Then burner-stabilized flamelets are computed, by decreasing the inlet mass flow rate. The properties of the flame

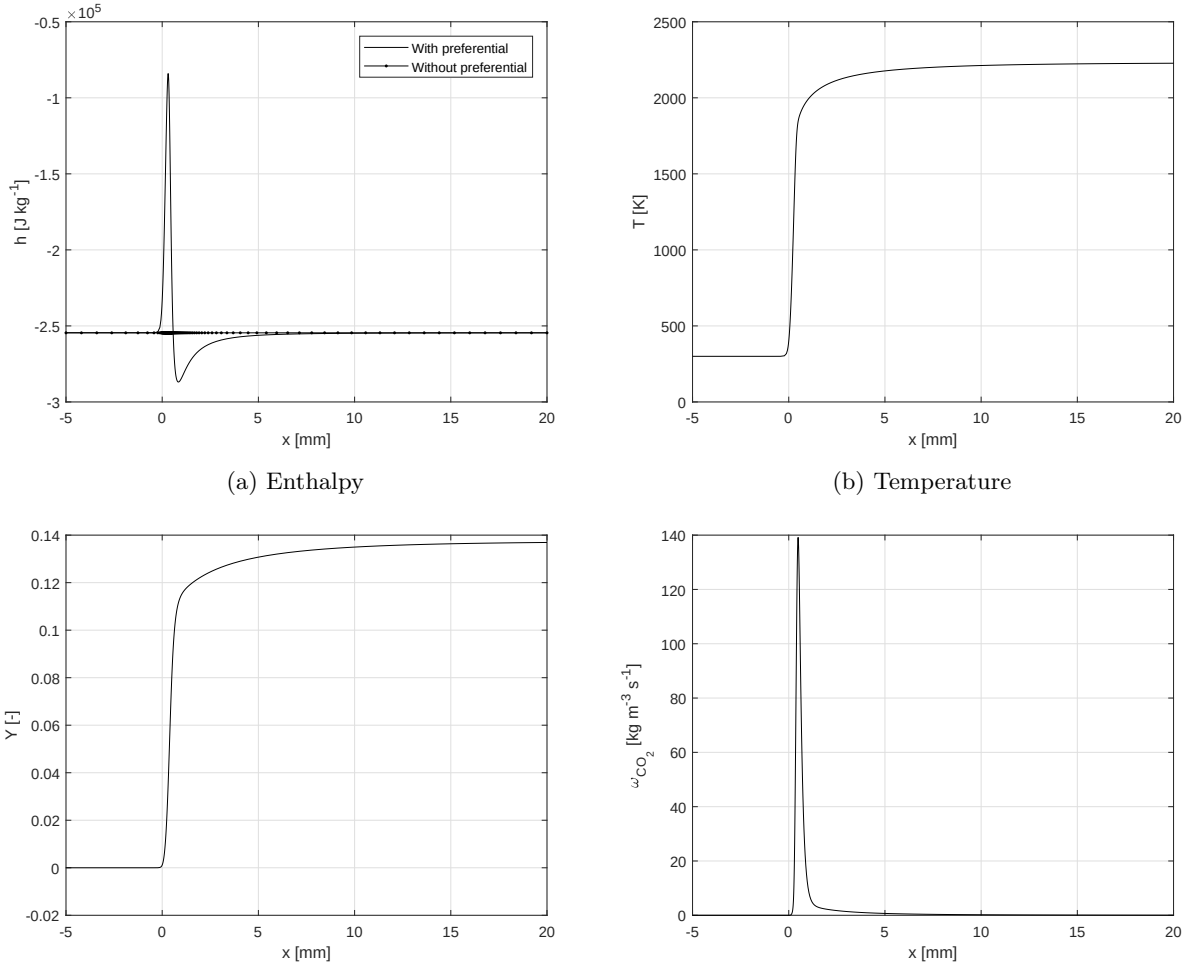

(a) Enthalpy

(b) Temperature

(c) Mass fraction progress variable (CO_2)

(d) Source progress variable (CO_2)

Figure 2.1: Adiabatic premixed methane/air flame for $\phi = 1$

structure are stored against the progress variable, $\mathcal{Y}_{CO_2}$, instead distance from the burner/flame front. When the variables are against progress variable, $\mathcal{Y}$, these values can be looked up according to the solution of progress variable, $\mathcal{Y}$. This way only one species equation ($\mathcal{Y}$) has to be solved, instead of solving for all species.

1D manifold

To construct FGM, the equations (2.39)-(2.41) are considered as adiabatic premixed flat flames. The boundary conditions at the burnt side are of Neumann type and at the unburnt side are of Dirichlet type. Figure (3.5) show, an example of one-dimensional manifold of an adiabatic flame, plotted against the distance from the flame front (x). Inlet temperature is considered to be 300K and an equivalence ratio of 1. It can be observed that in figure 2.1a, differential diffusion is neglected and considered to have constant enthalpy through the flamelet. This is done by considering the last value of burnt enthaply in a flamelet, as same at all points against progress variable/flame front.

2D manifold

In this section a two-dimensional manifold is constructed, to include enthalpy (h) variations to use it in FGM method for ionization chemistry in flames. To implement FGM method in CFD code, multiple flamelets are stored in the manifold with all variables. In one-dimensional manifold it is explained that differential diffusion is neglected, this is done for the simplification of the lookup and to reduce the computational time.

Initially for the construction of the two-dimensional manifold, a series of adiabatic, freely propagating flamelets are calculated, with varying inlet temperatures. Then flamelets are calculated by lowering the inlet massflow, which in turn decreases the enthalpy value of the flamelet. This way of calculation of the flamelets are done, by using burner stabilized flame type model. Adiabatic flamelets are calculated from initial inlet temperature of $T_u = 600K$ to $T_u = 250K$ in a step of decreasing 5K, where subscript u represents unburnt. Next enthalpy of the flamelets are decreased by varying massflow at the inlet by using burner stabilized flamelet model.

Figure (2.2a) show the manifold which includes both adiabatic and burner stabilized flamelets, and the extrapolation region. The manifold shown is created for premixed methane-air for an equivalence ratio of 1. Extrapolation of manifold is done by considering the coldest flamelet as shown in figure (2.2b). From this flamelet highest progress variable is kept constant, while initial progress variable value is extrapolated linearly as shown in figure. This measure is needed, for example when burnt gases are cooled intensively by heat sink. Due to this effect the enthalpy drops below that of the coldest flamelet. This method is effective in determining the data as no real flamelet is available at this region.

The domain of one-dimensional is considered from 0 to 2cm, and potential is applied at $x = L$ while keeping an zero potential at $x = 0$. For all the case L is considered to be 10cm. Figure (2.2c) show the source term of progress variable as a function of progress variable, shows the maximum production of CO_2 for various flamelets. Charged species (e^-) production rate are shown in figure (2.2d) and temperature in figure (2.2f), here solid lines show adiabatic flamelets while dashed lines show burner stabilized flamelets. It can be observed that temperature increases with increasing progress variable, this states that temperature is a function of progress variable and it is also true for enthalpy. This is also applicable for production rate of charged species, which can be observed from figure (2.2d). The applied electric field does not affect the production rate of charged species (which is explained in more detail in next chapter).

Figures (2.3) and (2.4) show the comparison of source progress variable, source and mass fraction of charged species, at two different applied potential of 0V and 20V. Figures (2.3a) and (2.3b) show source progress variable is independent of an applied potential. This also holds true for the production of charged species (e^-), from figures (2.3c) and (2.3c). However, the source term of charged species varies for an applied potential, as can be observed from figures (2.3e) and (2.3f). This suggests that the consumption of charged species is effected by an applied potential, as production is independent of an applied potential. Figures (2.4a) and (2.4b) show the distribution of mass fraction of charged species, for an applied potential of 0V and 20V. At an applied potential of 20V the maximum concentration of charged species is found near burnt region. As the electric potential is applied in the burnt region, electrons move towards an applied potential as they are attracted by the positive side. In summary it can be concluded that

$$\omega_{\mathcal{Y}} = f(\mathcal{Y}, h), \tag{2.42}$$

$$Y_{e^-} \neq f(\mathcal{Y}, h), \tag{2.43}$$

$$\omega_{e^-} \neq f(\mathcal{Y}, h), \tag{2.44}$$

$$\omega^+_{e^-} = f(\mathcal{Y}, h), \tag{2.45}$$

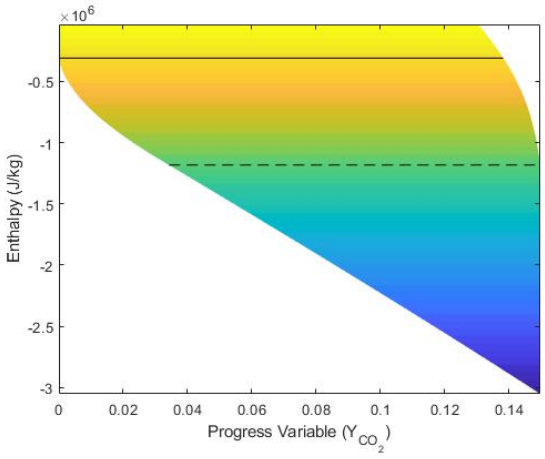

(a) 2D manifold with extrapolation

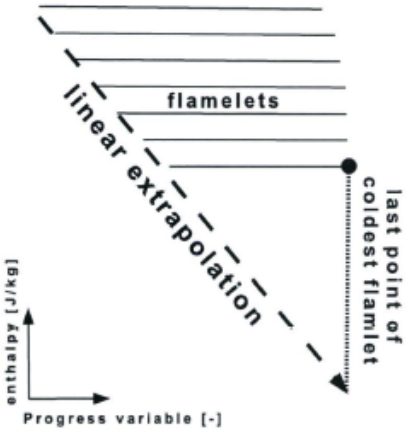

(b) Extrapolation of enthaply and progress variable [17]

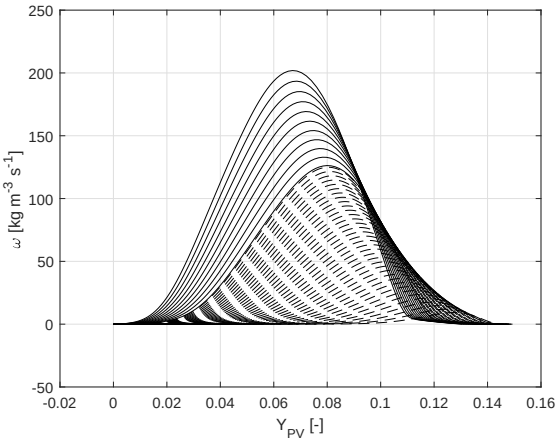

(c) Source progress variable

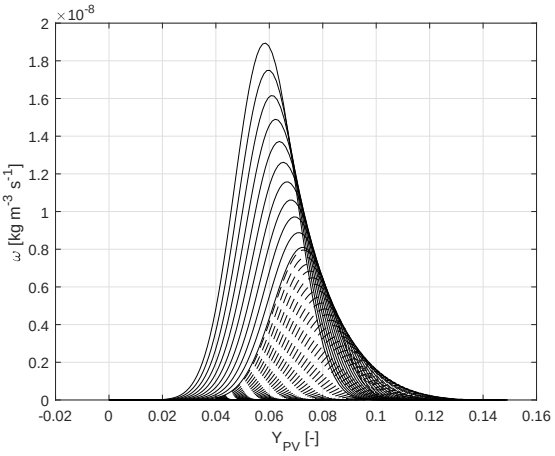

(d) Production of electron

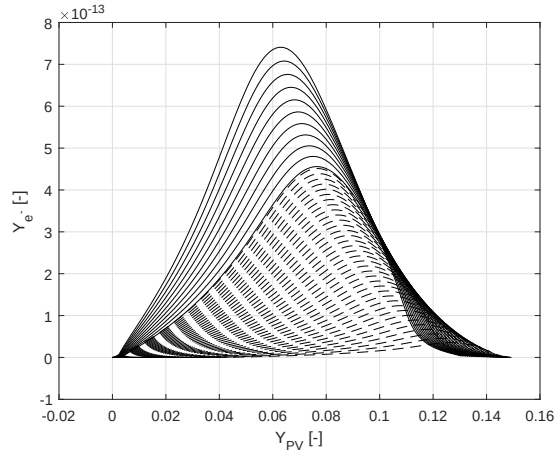

(e) Mass fraction of electron

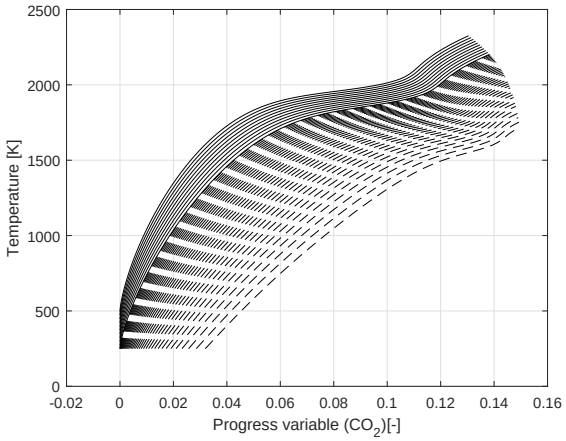

(f) Temperature

Figure 2.2: Figure (a) show the manifold where adiabatic flamelets are upto solid lines, while burner stabilized flamelets are upto dashed lines and the remaining region is extrapolated. Figure (b) show the method of extrapolation for enthaply and progress variable.

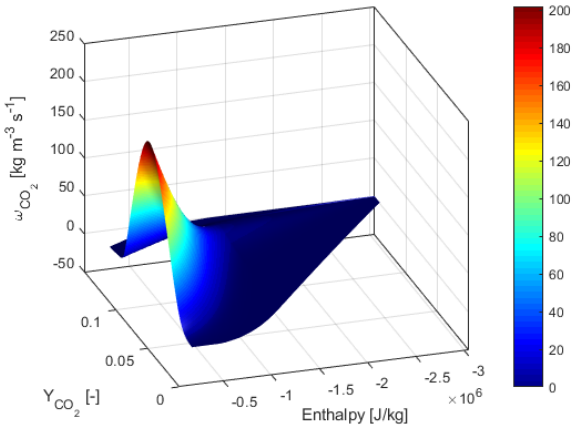

(a) Progress variable source term at 0V

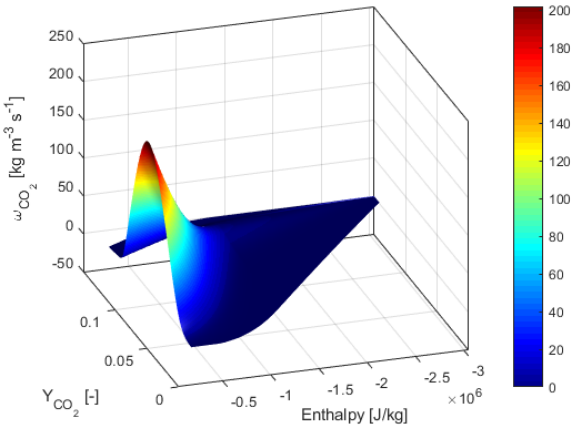

(b) Progress variable source term at 20V

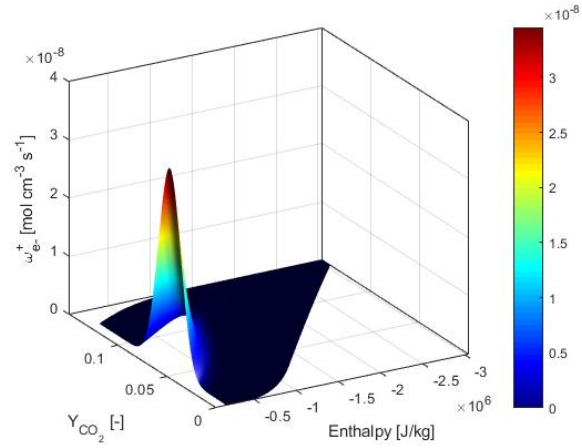

(c) Electron production at 0V

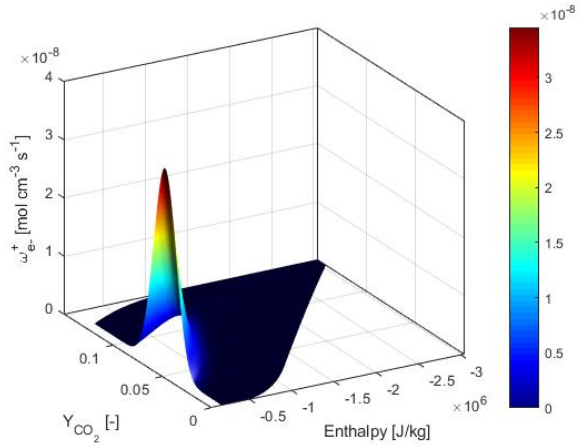

(d) Electron production at 20V

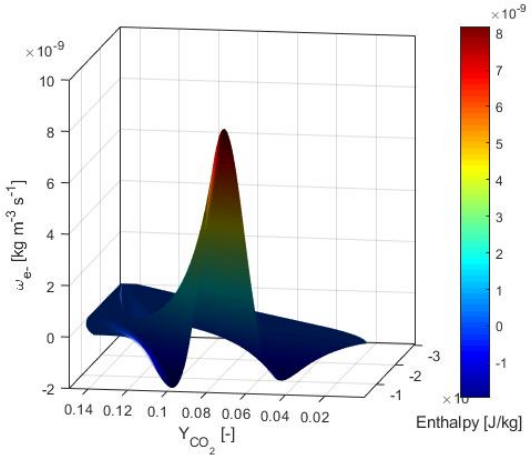

(e) Electron source term at 0V

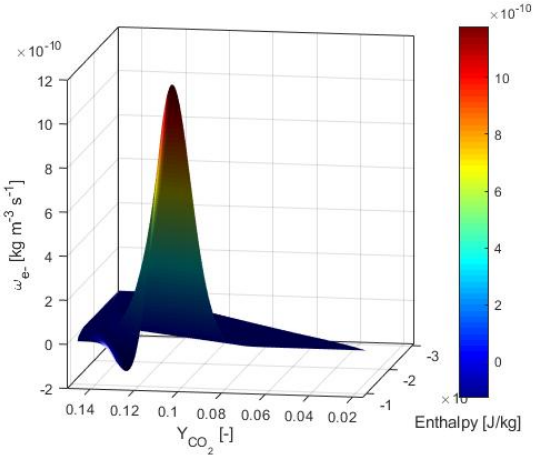

(f) Electron source term at 20V

Figure 2.3: Manifold of charged species at 0V and 20V and, progress variable as a function of enthalpy and progress variable.

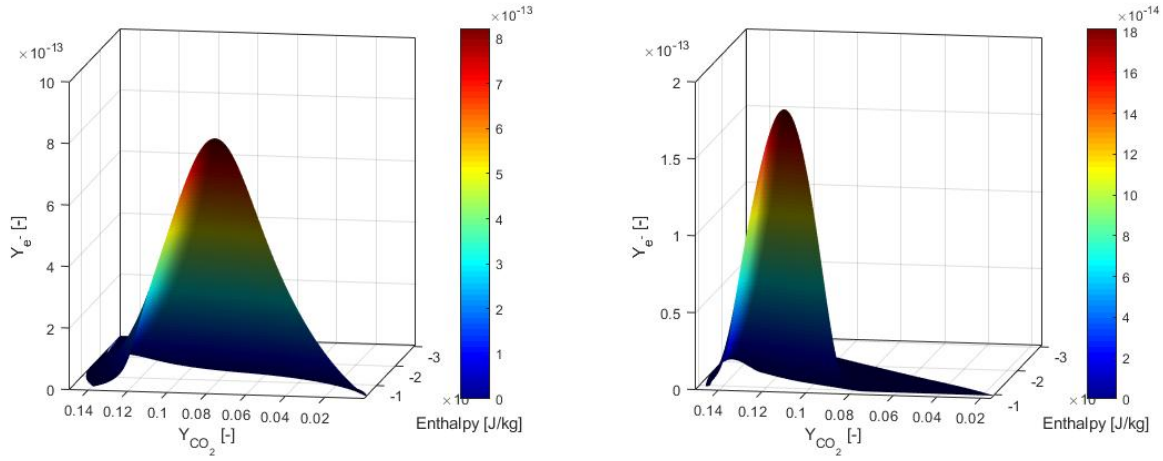

(a) Electron mass fraction at 0V

(b) Electron mass fraction at 20V

Figure 2.4: Manifold of charged species (e^-) mass fraction at 0V and 20V as a function of enthalpy and progress variable.

which means that the production rate of charged species and source term of progress variable are not effected by an applied external electric field. However, consumption rate and mass fraction of charged species are effected by an applied electric field.

2.5 Implementation of FGM method into CFD code

The conservation of mass and momentum are solved in the CFD code Ansys Fluent. These equations are given in equations (2.1) and (2.2). Additionally the energy equations which in this case the conservation of enthalpy and the conservation of progress variable are respectively given by

$$\frac{\partial \rho h}{\partial t} + \nabla \cdot (\rho \mathbf{v} h) - \nabla \cdot \left(\frac{\lambda}{c_p} \nabla h \right) = 0, \tag{2.46}$$

$$\frac{\partial \rho \mathcal{Y}}{\partial t} + \nabla \cdot (\rho \mathbf{v} \mathcal{Y}) - \nabla \cdot \left(\frac{\lambda}{Le_{\mathcal{Y}} c_p} \nabla \mathcal{Y} \right) = \dot{\omega}_{\mathcal{Y}}. \tag{2.47}$$

The enthalpy equation is only affected by an external heat sink and the diffusion term expressed in the progress variable equation is a function of the Lewis number $\mathrm{Le}_{\mathcal{Y}}$.

Using the FGM method, charged species (H_3O^+ and e^-) can be looked up from the table, but charged species are not just a function of progress variable when an external potential is applied as shown in figure 2.3 and 2.4. This makes it impossible to capture the effect of potential on charged species, when charged species are looked up by solving progress variable. Other method is to store charged species for all applied potentials. Then looking up charged species based on solution of progress variable, enthalpy (h) and electric field (E). This way of looking up is cumbersome and computationally expensive to create database for each potential, while this study is focusing on reducing the time to compute.

The best way to solve this problem is by solving additional transport equations for H_3O^+, e^- and potential. Since the production of charged species (ω^+) are independent of E, these are looked

up and the effect of electric field is also captured by solving potential equation. consumption of charged species are modeled based on the effect of potential on these species. So, this gives

$$\frac{\partial \rho Y_i}{\partial t} + \nabla \cdot \left[(\rho \mathbf{v} Y_i) - \left(\frac{\lambda}{Le_{Y_i} c_p} \nabla Y_i \right) + S_i \mu_i E \right] = \mathrm{M}_i(\omega_i^+ - \omega_i^-) \qquad i = \mathrm{H_3O^+}, e^-. \quad (2.48)$$

The production of charged species is computed as

$$\omega_i^+ = f(\mathcal{Y}, h) \qquad i = \mathrm{H_3O^+}, e^-. \quad (2.49)$$

The consumption is modeled as

$$\omega_i^- = k[\mathrm{H_3O^+}][\mathrm{e^-}], \quad (2.50)$$

$$\omega_i^- = k\ \rho \frac{Y_{\mathrm{H_3O^+}}}{\mathrm{M}_{\mathrm{H_3O^+}}} \rho \frac{Y_{\mathrm{e^-}}}{\mathrm{M}_{\mathrm{e^-}}}, \quad (2.51)$$

where k is the reaction rate constant is taken to be 2.88×10^{11} $\mathrm{m^3/mol\ s}$.

Chapter 3

Results of 1D simulations

In order to evaluate the diffusion model given in chapter 2, one-dimensional simulation results are compared for different diffusion models (Multi-component, mixture-averaged and constant Lewis). Then the effect of electric field on the charged species (e^- and H_3O^+) are studied and discussed, for different electrode distance and equivalence ratios. Furthermore, the chapter also discusses the validation of Flamelet Generated Manifold (FGM) method, with the detailed mechanism GRI 3.0 for varying external electric field.

The inlet temperature of the fuel-air mixture is maintained at 288K and pressure at 1bar. The equivalence ratio is taken to be 1, with inflow mixture mass flow rate of 0.0123 g cm^{-2} s^{-1}. This corresponds to an experimental methane flow rate of 1.733 slpm [27]. Flame type used in this case is burner stabilized flames, as they give realistic results when compared with experimental results.

3.1 Diffusion model comparison

In the previous chapter different diffusion models are given and formulated. In this section all three diffusion models are compared, with each other for detailed chemistry GRI 3.0, to see the accuracy of the diffusion models. First species mass fractions, temperature and enthalpy are compared for three diffusion models, with and without applied external field. Applied potential consists of saturation and non-saturation conditions for electric fields. Then the charged species are compared for the same boundary conditions considered.

3.1.1 Without applied electric field

Figure (3.1a) show the mass fraction of major species and figure (3.1b) show the mass fraction of CH and O for different diffusion models. The major species contributing for chemi-ionization reaction CH and O, mass fraction are same for all three diffusion models. Figures (3.5d) and (3.1d) show temperature and source progress variable against the distance from the burner. The maximum temperature difference is calculated to be 8K for considered diffusion models. This is a small difference which is acceptable. So, the figures show that all three models are in good agreement with each other in terms of species, temperature and source terms.

Now for the same boundary conditions, charged species with constant Lewis and mixture-averaged diffusion models are compared with multi-component diffusion model. Figures (3.2a) and (3.2b) show mass fractions and production, and consumption of the charged species. It can be observed that mass fraction of charged species of both diffusion models compare well with multi-component diffusion model. The peak production value of charged species from constant Lewis and mixture-averaged models, deviates 1.7% and 2.3% when compared with multi-component model. Whereas, production value of charged species from constant Lewis and mixture-averaged models, deviates 1.6% and 2.3% when compared with multi-component model. This suggests that both constant Lewis and mixture-averaged model predicts well when compared with multi-component model for charged species.

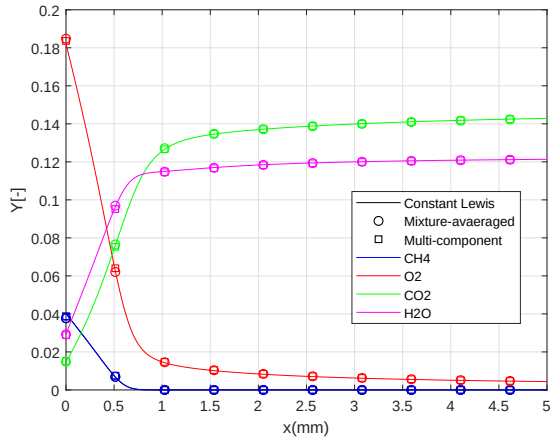

(a) Species mass fraction

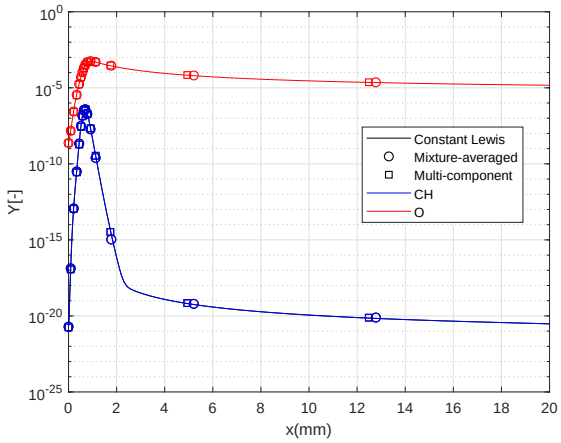

(b) CH and O distribution

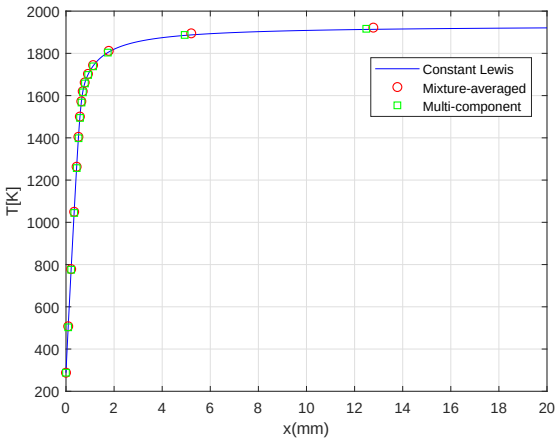

(c) Temperature distribution

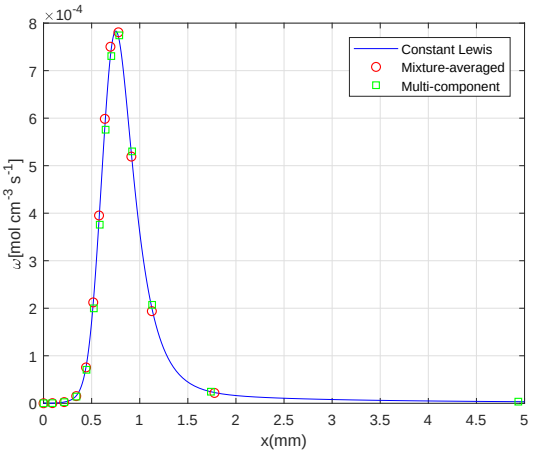

(d) Source progress variable (CO_2)

Figure 3.1: Species mass fraction, temperature and source progress variable are plotted against distance from the burner for all three diffusion model. With inlet temperature taken to be 288K, equivalence ratio (ϕ) = 1 for burner stabilized flame.

3.1.2 With applied electric field

To compare the effects of the diffusion model due to an external applied potential, two cases are considered; non-saturation (20V) and saturation (100V) conditions. Figure (3.3) show that the

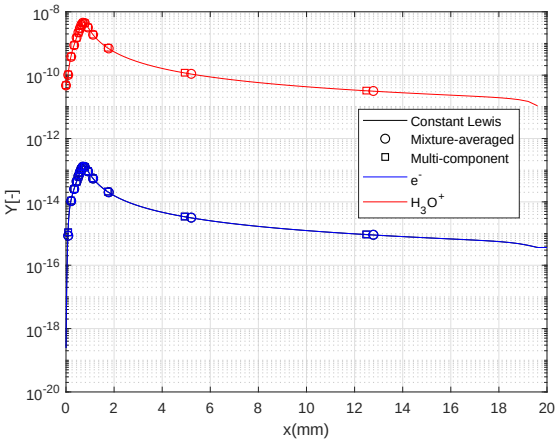

(a) Charged species mass fraction

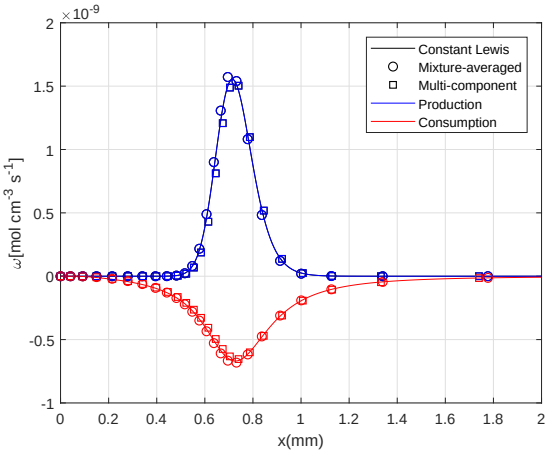

(b) Production and consumption of charged species

Figure 3.2: Charged species mass fraction and source without applied external electric field, for three diffusion models.

effect of an applied electric field on the charged species source for both, constant Lewis and mixture-averaged diffusion models are in good agreement with the multi-component diffusion model. The electric field does not have an effect on the production of charged species, but the consumption reduces to zero with increasing potential. This is expected due to the attraction of charged species to its opposite polarities which causes charge separation.

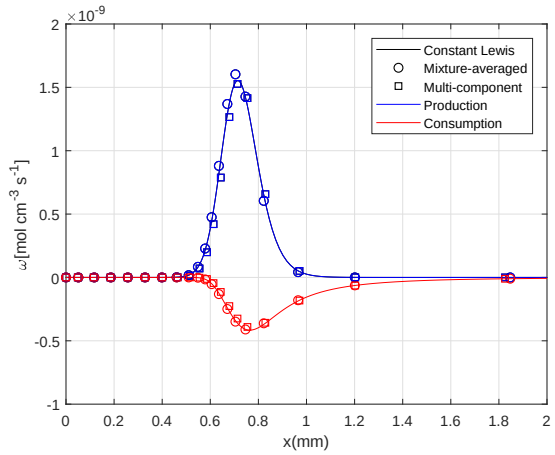

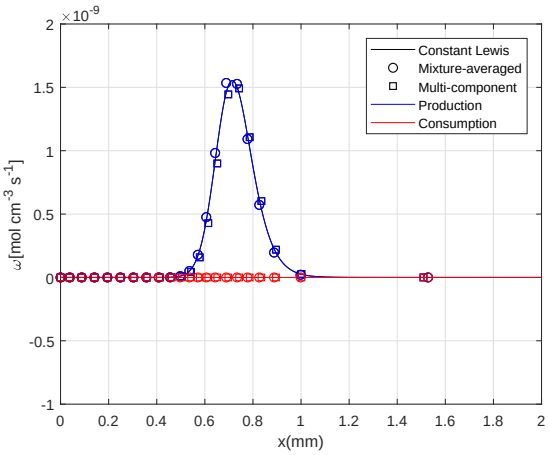

Figure 3.3: Left and right figures show production and consumption of charged species for 20V and 100V respectively.

For saturation potential, production rate of charged species for constant Lewis and mixture-averaged diffusion models have 1.7% and 2.3% deviation from multi-component model respectively. This deviation is similar compared to zero applied potential from above case. For the non-saturation condition, consumption of charged species have 2.7% and 3.3% deviation respectively. This suggests that all three diffusion models, have the same effect on the distribution of charged species for an applied electric field. As the use of constant Lewis numbers is simpler and faster, this model is used from hereon to compute charged species.

3.1.3 Electric current

One of the main objectives of this study is to determine the electric current due to the effect of a potential on charged species. In order to achieve this, a current comparison should be done for different diffusion models, keeping multi-component as reference. Figure (3.4) show the current measured against an applied potential from 0V to 100V for all diffusion models. It can be observed that both the constant Lewis and mixture-averaged diffusion models compare well with the multi-component diffusion model. For all diffusion models the electric current saturates above 80V applied potential. As the constant Lewis diffusion model compares well with the diffusion model and it is computationally less intensive as well. Constant Lewis diffusion model will be used from hereon and for all simulations.

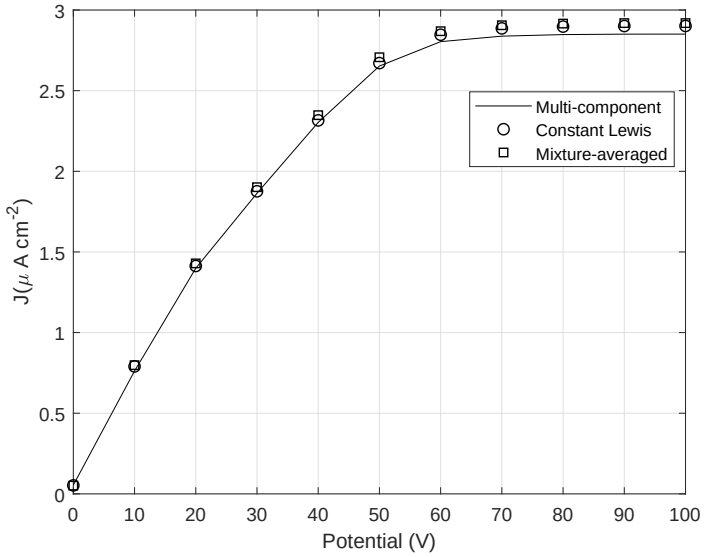

Figure 3.4: Current comparison for all three diffusion models.

3.2 Influence of electric field

Before studying the effect of electric field on charged species, first let's look at how it affects the flame properties and major species. In order to distinguish between the effect of electric field on major species, flame properties are compared for an applied potentials of 0V and 50V. Figure (3.5a) show the distribution of major species along the flame, with solid lines representing the 0V and circles representing 50V applied potential. Figure (3.5b) show the reaction zone zoomed in and figure (3.5c) show minor species CH and O mass fraction with both x axis limited to 5mm. Production and consumption of CH happens quickly while O concentration decreases along the flame. Overall it can be noticed that there is no effect on the major or minor species by application of a potential. Figure (3.5d) show temperature distribution and this is also not effected by an applied potential. This suggests that the external potential does not have an effect on neutral species and temperature distributions.

To see the effect of the electric field on charged species behavior, a constant Lewis diffusion model is considered as explained above. Effect of potential on charged species are studied for various electrode distance and different equivalence ratio. The effect of electric field is discussed for zero

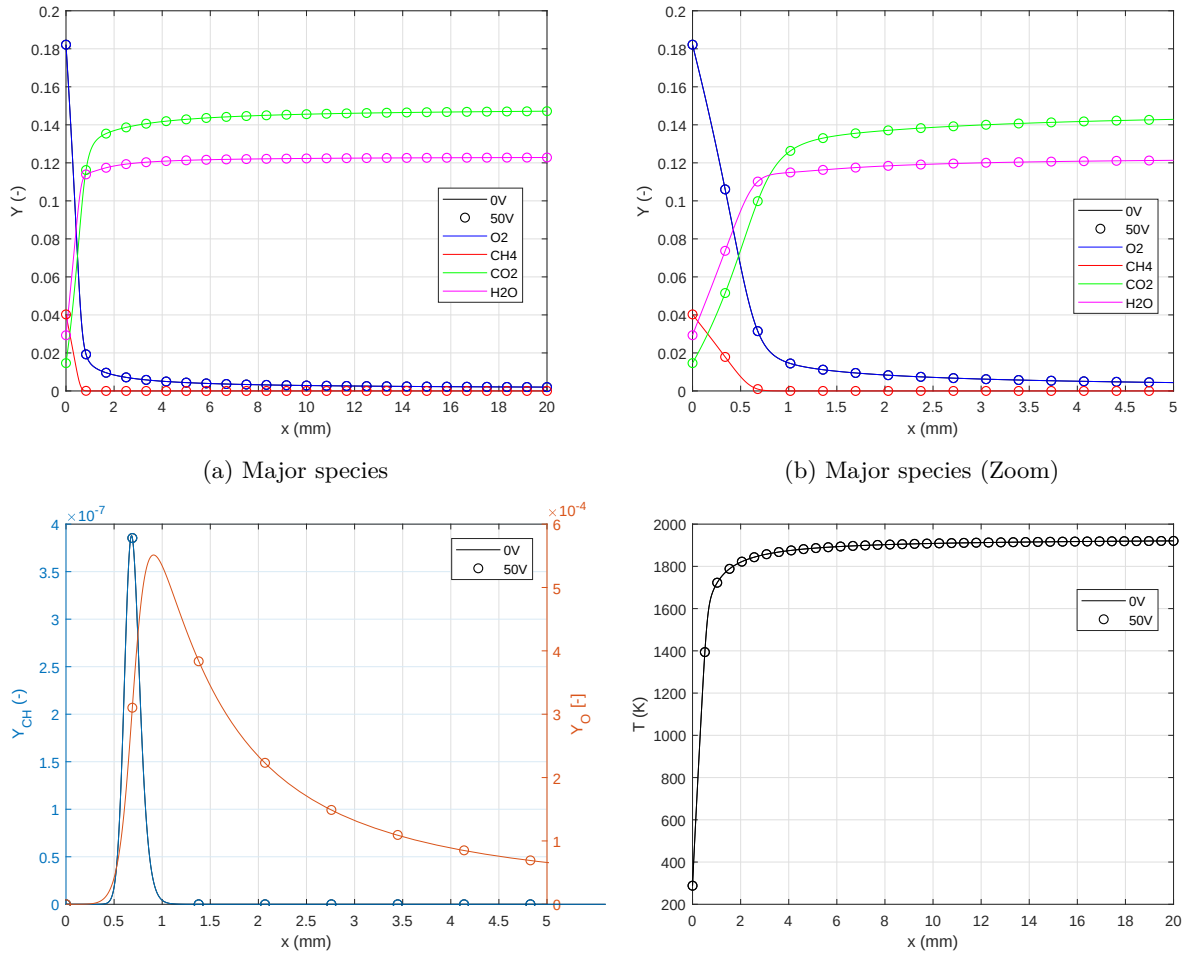

(a) Major species

(b) Major species (Zoom)

(c) Mass fraction of CH and O (Zoom)

(d) Temperature

Figure 3.5: Major species, temperature, CH and O mass fraction comparison for with and without applied potential.

applied external potential, non-saturation and saturation electric field.

3.2.1 Electrode distance

In this section the effect of the electric field on charged species are discussed for different electrode distances, which are 3.7mm, 10mm and 20mm from the burner deck of the heat flux burner. For each of this case, three different external electric field is considered and its effect on charged species is studied and discussed. To visualize the effect of potential, the x axis is limited to 2mm from the burner. It can be observed from figure (3.6a) that for zero potential, production and consumption of charged species are not affected which is expected. This is due to the internal electric field which keeps charged species together.

Figure (3.6b) show the effect of an applied potential on charged species for 20V. For the same potential at all electrode distance, the consumption of charged species varies while production remains the same. At 20V applied potential, increasing the electrode distance decreases the

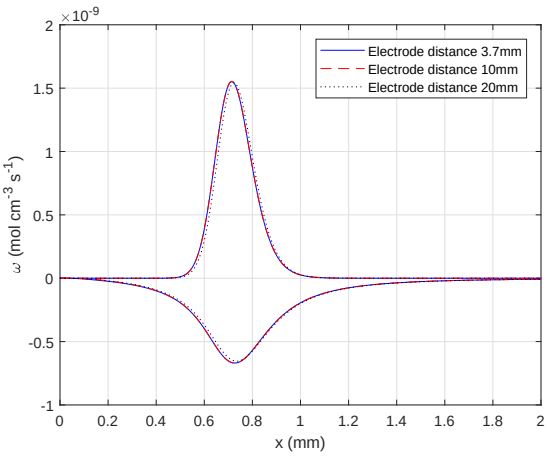

(a) Without applied electric potential ($\Delta\Phi = 0$)

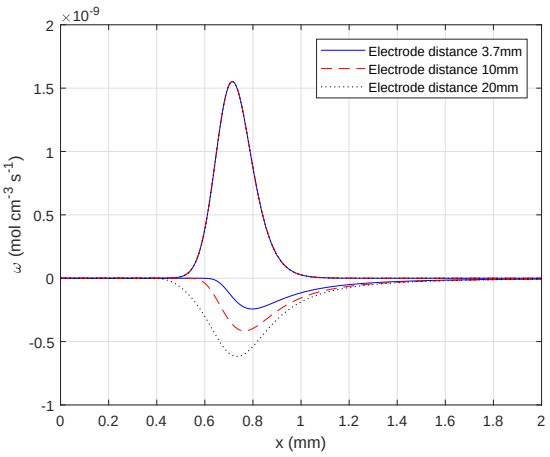

(b) Applied electric potential of 20V

Figure 3.6: Influence of applied external potential for various electrode distances for zero applied potential and non-saturation electric field. Positive source plot represents the production rate while negative source plot represents the consumption rate.

electric field force. This leads to decrease in the electric force for charge separation of charged species, which leads to lower consumption rate of charged species as electrode distance increases.

Now considering an applied potential of 100V, which is shown in figure (3.7a). At an electrode distance of 20mm, there is still recombination reaction/consumption of charged species, whereas for the other two electrode, distances the consumption of charged species is almost zero. This is explained due to the smaller electric force on the charged species near the flame front. For the electrode distance of 20mm it takes twice the potential to reach the saturation condition, this is shown in figure (3.7b). This suggests that increasing the electrode distance will need higher potential to achieve saturation condition.

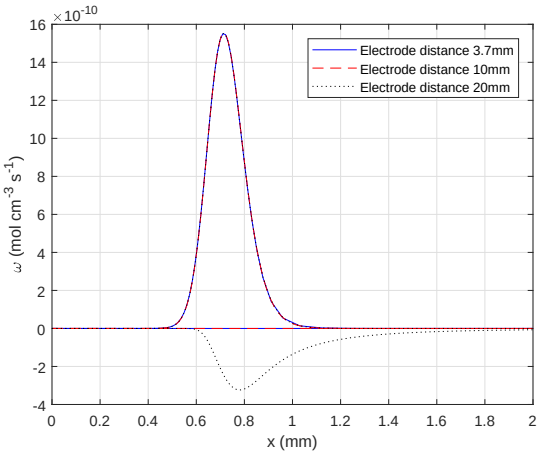

(a) Applied electric potential of 100V

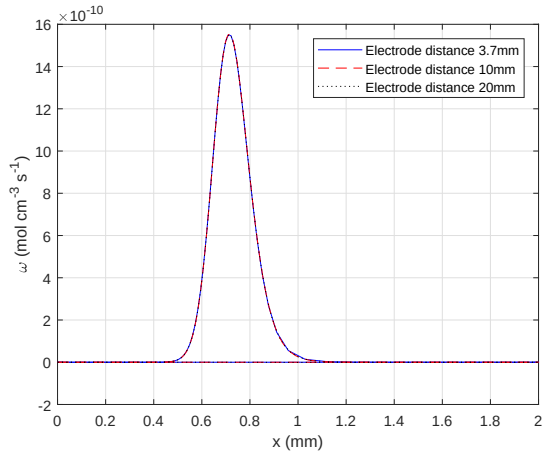

(b) Applied electric potential of 200V

Figure 3.7: Influence of applied external potential for various electrode distances for saturation electric field.

3.2.2 Equivalence ratio

In the previous section the effect of potential is discussed, for different electrode distance from the burner. An electrode distance of 10mm is considered to analyze the effect of external potential, as this doesn't affect the flame front due to the heat loss effect, and also saturates at lower potential. Considering the 10mm electrode distance, and by changing the equivalence ratio from lean to rich and the concentration of charged species are studied.

Figure (3.8a) and (3.8b) show the production and consumption of charged species, at an applied external potential of 0V and 20V respectively for various equivalence ratios. The source of charged species increases with increasing equivalence ratio (from 0.8 to 1.0), this is expected as increasing the equivalence ratio increases the concentration of hydrocarbons. This leads to higher concentration of charged species from chemi-ionization reaction. There is a less production and consumption of charged species for rich mixture. This is caused due to insufficient oxygen for the combustion and also decrease in temperature, which affects the production of charged species.

At an applied potential of 20V, lean mixture of 0.8 equivalence ratio attain saturation where consumption of charged species is zero. This is due to the lower production of charged species compared to equivalence ratio of 1. It can be concluded that lean mixture attend saturation at lower potential due to less source term of charged species in the reaction.

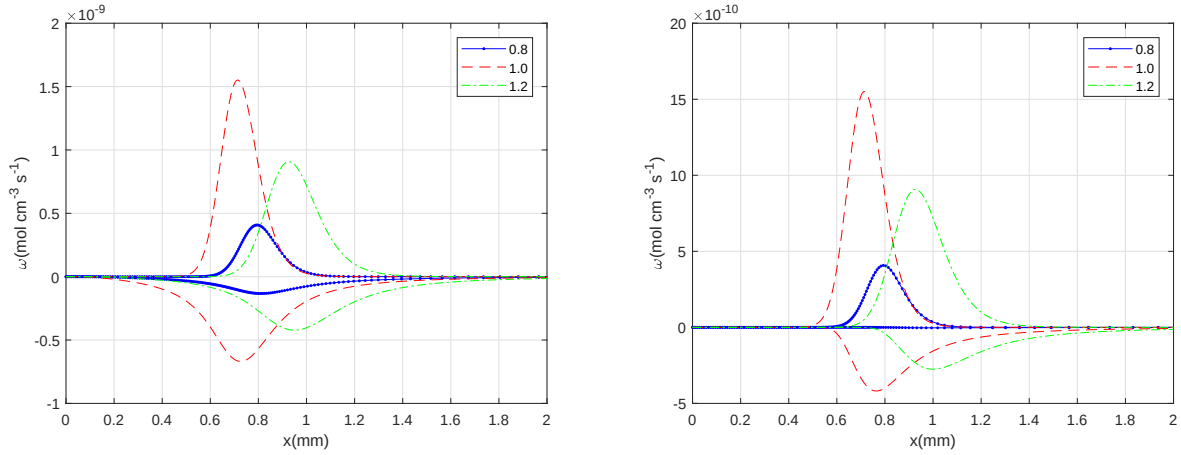

(a) Source at 0V

(b) Source at 20V

Figure 3.8: Charged species mass fraction and source with and without applied external potential for various equivalence ratio.

3.2.3 Current comparison

Figure (3.9a) show a comparison of current for different equivalence ratios and electrode distances. The saturation current is different for different equivalence ratios. In rich fuels due to less oxygen, leads to less production of charged species which in turn leads to less current density. It is also important to notice that the saturation currents are also different for different electrode distances. As the electrode distance increases, electric force should also increase as the charged species needs to travel a larger distance.

Simulated and experimental current are compared for all three electrode distances for an equivalence ratio of 1 in figure (3.9b). The experimental saturation current for all electrode distance is

70μA, while simulated saturation current is 80μA. The numerical result is able to correctly predict the behavior of the current for all electrode distance.

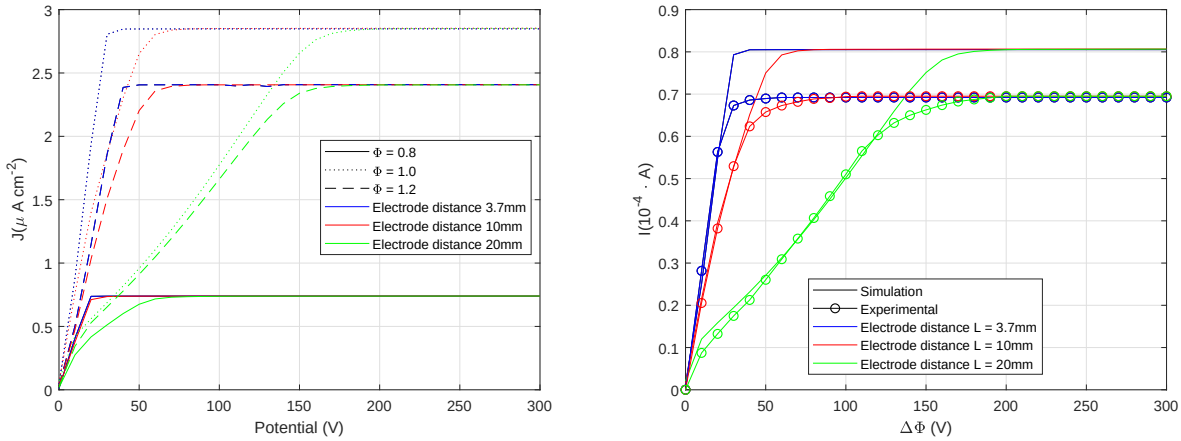

(a) Different equivalence ratios

(b) Equivalence ratio of 1

Figure 3.9: Current comparison are for three electrode distances. Right figure show the current comparison with experimental results.

3.3 FGM validation

Before analyzing the 2D FGM results, we will first investigate how FGM compares against 1D detailed chemistry for ionization reaction and applied potential. In this section the FGM method is validated against detailed chemistry with and without an applied external potential. First boundary conditions considered for this validation are given, then a comparison of major species with detailed chemistry without applied external potential. Further, charged species source terms are compared with and without an applied external potential.

3.3.1 Settings and conditions

For all conditions the inlet temperature is maintained at 288K and the pressure at 1bar. In the previous section the effect of an external potential on charged species for different electrode distances is discussed. In this case the electrode distance is maintained at 10mm from the burner, having a smaller electrode distance might affect the flame structure when heat loss is given to electrode and larger distance will lead to higher potential for saturation of consumption of charged species.

The FGM database contains flamelets with 300 grid points in both enthalpy and progress variable (CO_2) direction. This is in order to capture charged species profile, mainly electrons which are very sensitive to applied potential. For this validation, the equivalence ratio is taken to be 1 with an inflow mixture mass flow rate of 0.0123 g cm^{-2} s^{-1} corresponding to an experimental methane flow rate of 1.733 slpm.

3.3.2 Validation of FGM results for charged species

Before proceeding to compare charged species first, let have a look at how well FGM method computes major species, temperature and progress variables with detailed results. Figure (3.10) show comparison of the FGM method with the detailed chemistry results, computed by CHEM1D software. It can be observed from figures (3.10b) and (3.10d) that, the FGM method reproduces the results obtained by CHEM1D very well with detailed chemistry for major species and temperature respectively.

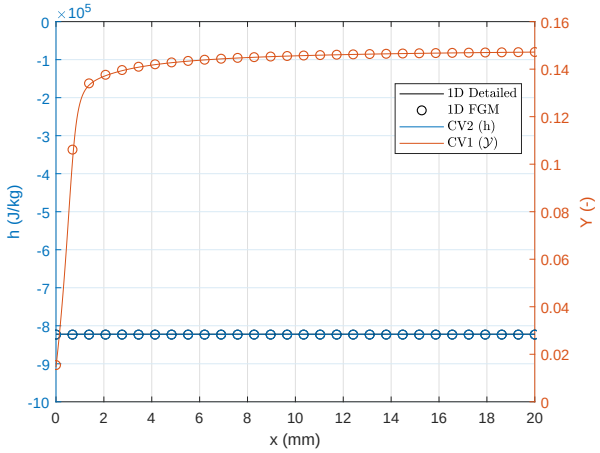

(a) Enthapy and progress variable

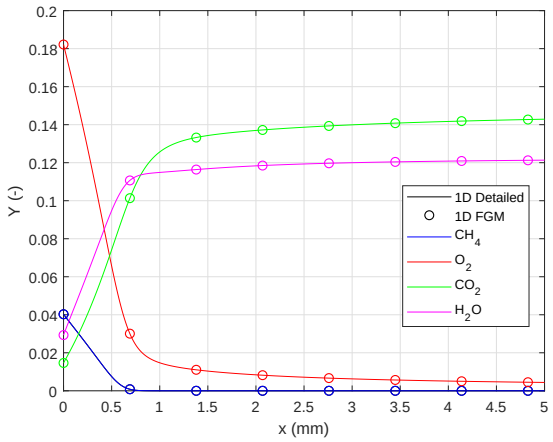

(b) Major species

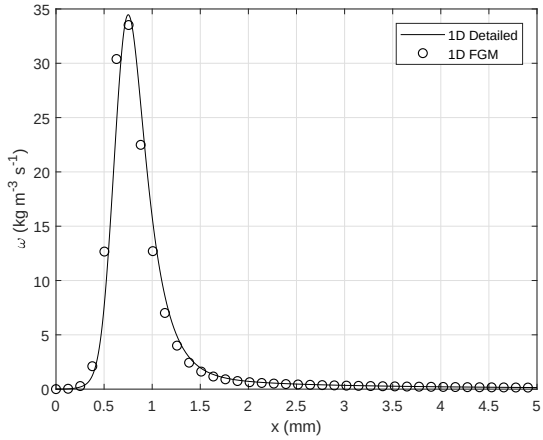

(c) Source progress variable

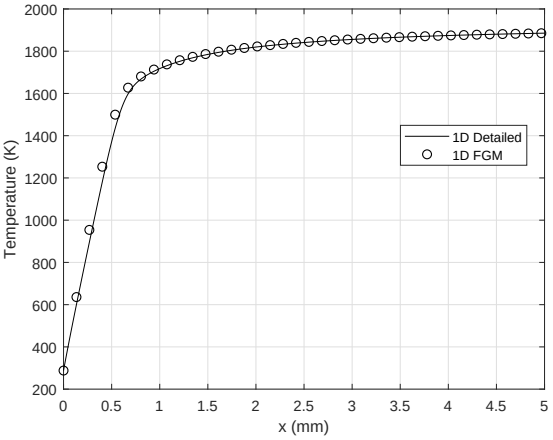

(d) Temperature

Figure 3.10: Comparison of FGM method against detailed chemistry in one-dimensional, where CV1 and CV2 represent progress variable (CO_2) and enthalpy respectively. The x-axis limit is taken to be 0 to 5mm.

In two-dimensional FGM implementation there are a total of five transport equations that are solved, in which progress variable and enthalpy are included. So, it is important to validate how these two compare with detailed results. Figure (3.10a) show FGM results compared with detailed results. It can be noticed that, both mass fraction of progress variable and enthalpy compares well with detailed results. Figure (3.10c) show a comparison of source progress variable with detailed chemistry, this also compares well with the detailed result. This show that the FGM method compares well with detailed chemistry for major species.

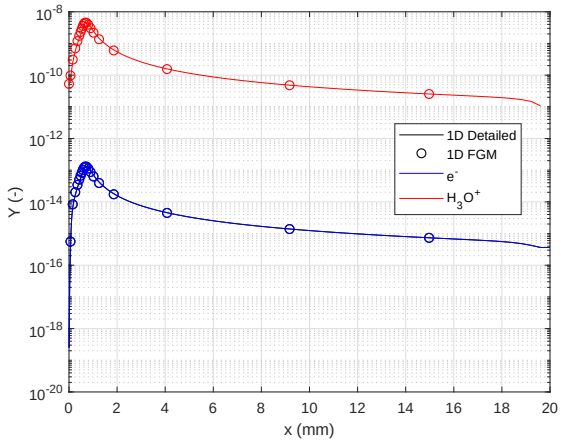

(a) Charged species mass fraction ($\Delta\Phi = 0$)

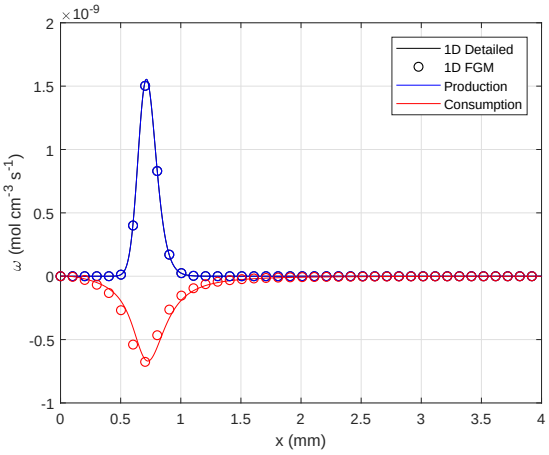

(b) Source charged species applied potential $\Delta\Phi = 0$

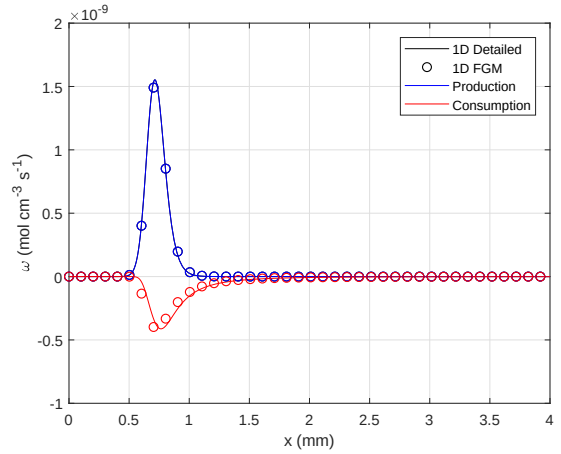

(c) Source charged species at applied potential of 20V

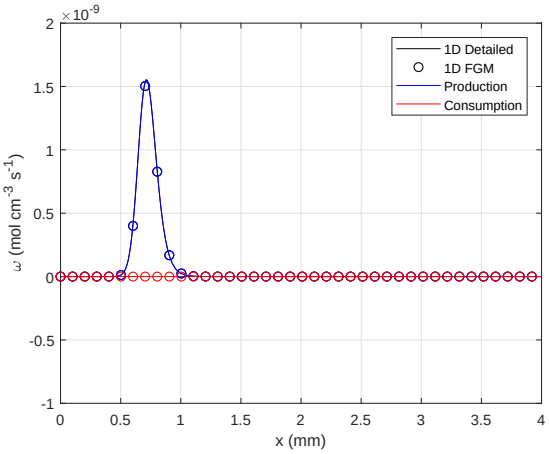

(d) Source charged species at applied potential of 100V

Figure 3.11: Comparison of FGM method against detailed chemistry in one-dimensional of charged species for various applied potential. Electrode is at a distance of 10mm from the burner, x-axis is limited to 4mm for source of charged species (e^-) plots.

As this study is about the effect of an external potential on charged species, it is important to validate the charged species FGM results with detailed chemistry. As explained in Chapter 2, instead of looking up the charged species from an FGM database, transport equations are solved for both e^- and H_3O^+ including the potential equation. As the database is created without an external applied potential, looking up the charged species will result in the same values for a changing potential. To capture the effect of the electric field on the application of an electric field, transport equations are solved for the charged species and potential. Production of the charged species are looked up by solving equation (2.49), where it is a function of progress variable and enthalpy. As the production rate is not effected by an electric field, the consumption rate is computed by equation (2.51), as it is a function of an applied electric field. Solving this way, captures the effect of an electric field on the charged species and also requires a single database with no applied potential.

Figures (3.11a) and (3.11b) show mass fraction and source of charged species for no applied external potential. Both mass fraction and production of charged species compares very well with detailed results, this is expected as production of charged species are looked up from the table. Even

the consumption of charged species compares well with the detailed results, this makes the FGM method reliable for computing charged species. Figures (3.11c) and (3.11d) show the sources of charged species for applied potential of 20V and 100V, from these it can be concluded that FGM predicts well for both the production and consumption of charged species compared to detailed results. This suggests that the FGM method computes consumption of charged species very well with and without an applied potential.

3.3.3 Current validation

One of the important parameter to check, is the electric current calculated by the FGM method. This is compared with the detailed study using the constant Lewis diffusion model. Figure (3.12) show the comparison of electric current for the FGM model and detailed model in one-dimensional results. To compare this for an equivalence ratio of 1, the applied potential is varied from 0V to 100V. It can be observed that the current computed by the FGM model has a good-correlation with the detailed result. At an applied potential above 70V the current saturates, which is caused by the strong electric field that enables recombination of charged species impossible, leading to a maximum current for that equivalence ratio.

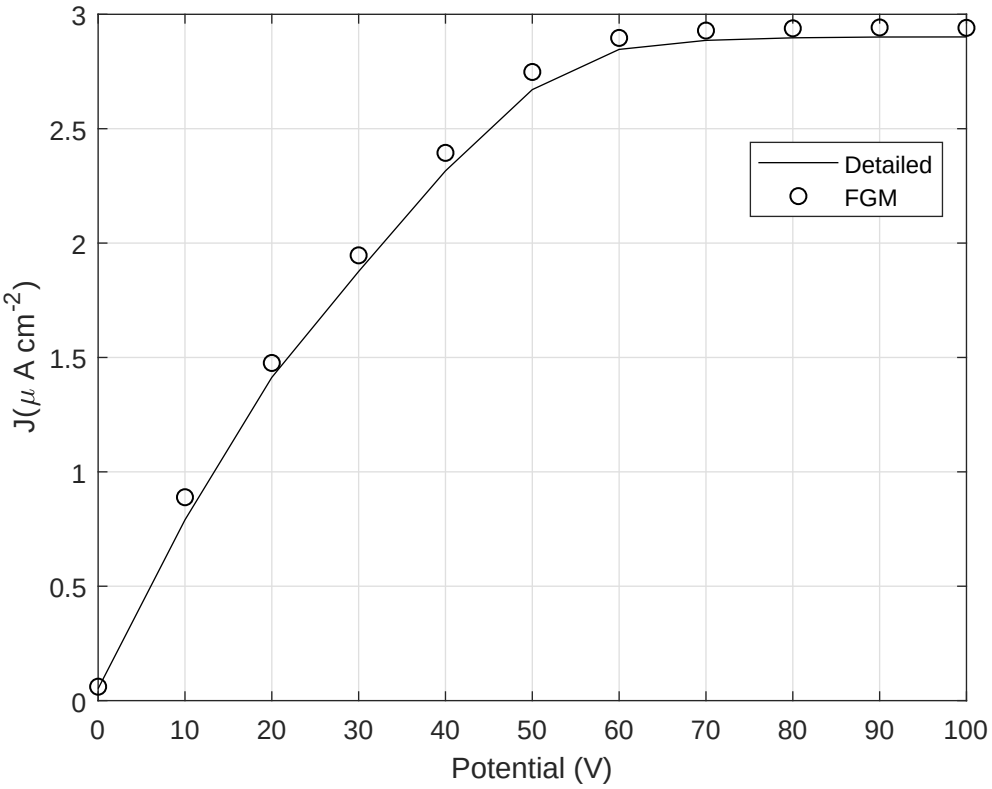

Figure 3.12: FGM current validation against detailed results for an equivalence ratio of 1.

3.4 Conclusion

Charged species are formed because of the chemi-ionization reactions in a flame. During this process, different positive and negative ions are formed but this study only accounts for H_3O^+ and e^- to make the computation simpler. The concentration of these species are studied and it is concluded that both are equal due to proton transfer reaction, where all CHO^+ quickly reacts with H_2O to give H_3O^+. To make the computation less intensive, different diffusion models are studied and found that all models shows good results with multi-component diffusion model. This is studied for both with and without applied external electric field. As constant Lewis model is less intensive for computation it is considered for calculation purpose.

Further in this chapter, the effect of electric field on charged species are studied, by varying the electrode distance and equivalence ratio and are reported. For separation of charged species, the electrode distance plays an important role for an applied potential. Increasing the electrode distance leads to less charge separation due to less electric force at an applied potential. To reach saturation current for an electrode distance of 20mm, it takes twice the applied potential than for the electrode distance of 10mm. The FGM model comparison is also studied and compared with detailed results. For different applied electric potential, the FGM results validates well with detailed results for all conditions.

Chapter 4

Results of 2D simulations

In the previous chapter the effect of an electric field on charged species are studied and reported, including the validation of FGM method with the detailed chemistry in one-dimensional flames. To extend it further, in this chapter a two-dimensional model is considered and the FGM method is used, to solve a two-dimensional flat flame using Ansys Fluent software. The obtained result is then compared with one-dimensional detailed chemistry results, as two-dimensional detailed chemistry is computationally expensive this wont be studied in here.

This chapter focuses on the two-dimensional model description and boundary conditions are given. The FGM method is studied for two-dimensional geometry for ionization mechanism in flat flames using the heat flux burner. This is studied with and without an applied external potential field and the results are discussed. Further, mesh adaptation is studied and quality of the results are discussed.

4.1 Model description

The Heat Flux Burner (HFB) is modeled with a two-dimensional geometry and it is used to simulate flat flames. Figure (4.1) show the HFB in a two-dimensional geometry, and the electrodes used to apply an external potential. Table (4.1) show the dimensions used for the two-dimensional HFB. The inlet of the burner is taken to be 0.5mm, while the burner width is 0.2mm. The electrodes are at a distance of 10mm from the burner deck, with a diameter of 1mm. This model has a maximum width of 1.4mm, with an electrode and two inlets for premixed methane-air mixture. As the model is a small section of the HFB, the vertical lines are considered to be symmetric. All the dimensions are considered are given in the table.

The model is meshed using a quadrilateral face mesh in the entire geometry. This has an advantage over the use of triangular mesh as quadrilateral mesh lowers the skewness, which improves quality and convergence by reducing the errors in Ansys Fluent. Skewness and orthogonality ranges from 0 to 1, where a value close to 1 corresponds to low quality for skewness and value close to 0 corresponds to low quality for orthogonality. Maximum skewness for the considered mesh is 0.18 while orthogonality is 0.82.

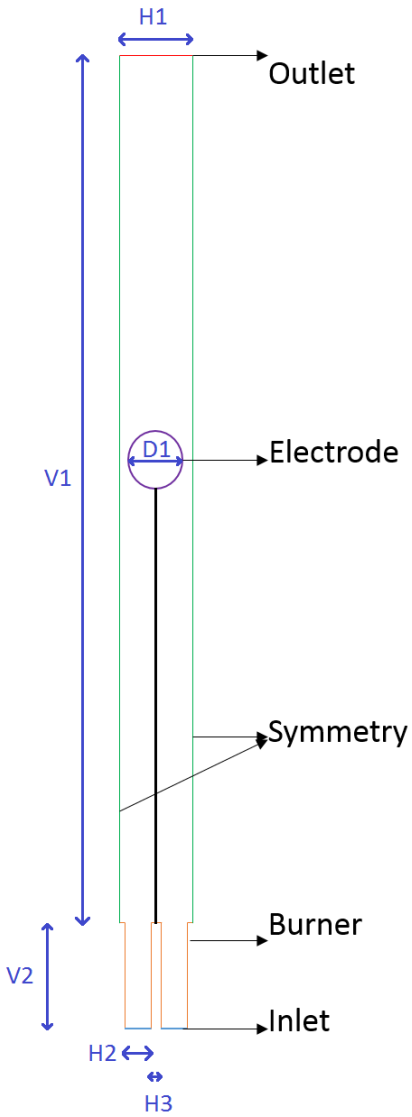

Figure 4.1: Segment of Heat Flux Burner used for simulations.

Name	Dimension[mm]
V1	20
V2	2
H1	1.4
H2	0.5
H3	0.2
D1	1

Table 4.1: Dimension of Heat Flux Burner.

4.1.1 Boundary Conditions

The solver used here is the pressure-based steady state solver to solve for flat flames with laminar viscous model. To compare with the experimental results from [27], inlet velocity at the HFB burner is taken to be 0.153 ms^{-1}, which corresponds to an experimental mass flow rate of 0.0123 g cm^{-2} s^{-1} with an inlet temperature of 288K. In reality no flame is adiabatic, so in order to stabilize the flat flame above the burner, a temperature of 300K is maintained at the burner. Properties like diffusivity, density and viscosity are read from the database using the Fluent UDF.

As already mentioned in chapter 1, five user defined scalars (transport equations) are solved in this study. It includes enthalpy, progress variable, potential, positive ion (H_3O^+) and electron (e^-) concentration. All transport equations used are solved using a second-order upwind scheme, this is preferred over the first-order upwind scheme. As the second order upwind scheme includes 3 data points, instead of 2 data points. This results in more accurate result for the approximation of spatial derivative.

4.1.2 Grid convergence

To study the grid independence and to find the best suitable course mesh, four different mesh sizes are considered, with varying cell sizes from course mesh (0.1mm) to fine mesh size (0.025mm) as shown in table (4.2). To verify the best suitable mesh, figure (4.2) show a comparison of temperature for various mesh sizes. It can be observed from figure (4.2b) and table (4.2) that of both the course and medium mesh, predicts higher temperature while the fine mesh has a good approximation for the detailed results.

The fine mesh has approximately 50,000 cells and this makes the computation CPU intensive. In order to reduce the computational time and to keep the accuracy of the solution, region adaptation of the mesh is considered. In the reaction zone the density of the mesh is increased. Since the study is mainly focused on the ionization mechanism, the region considered for mesh adaptation is 0mm to 2mm from the burner.

Mesh adaptation for maximum temperature has a better agreement with the detailed study. Also from figure (4.2b) it can be noticed that for the burnt region adaptive mesh has a better agreement with the detailed result. As the adaptive mesh model has less than half the number of cells, computational time also decreases which makes this model effective for computation. So, the mesh considered for the computation is region adapt.

Type	Node	Face	Cell	Size [mm]	Max Temp [K]
Course	3207	6145	2938	0.1	1915.3
Medium	12262	23986	11724	0.05	1915.3
Fine	47896	94718	49822	0.025	1906.3
Adapt	21725	42756	21031	0.025-0.05	1907.6
1D	-	-	-	-	1908.5

Table 4.2: Properties of mesh considered for the grid convergence and maximum temperature is compared with the detailed result.

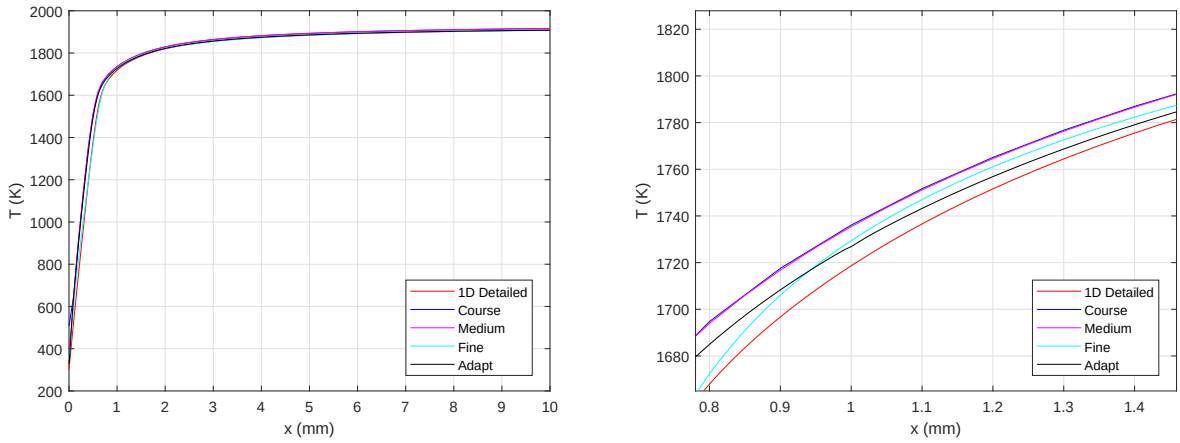

(a) Temperature

(b) Temperature

Figure 4.2: Temperature plot for various mesh size to study grid convergence.

4.2 Results

In this section the FGM method is used to solve flat flame in Ansys Fluent. First, a flat flame is solved without applying an electric field and its flame characteristics are compared with one-dimensional detailed results obtained from CHEM1D. Then, the results including application of external potential are discussed.

To compare simulated two-dimensional FGM results with one dimensional detailed results, a line from the burner to the electrode is considered as shown in figure (4.1). Figures (4.3a) and (4.3c) show progress variable mass fraction and source term respectively. FGM result matches well with the detailed result obtained from CHEM1D, there is a slight deviation before 0.5mm which is due to enthalpy change due to the temperature being different from burner to inlet which causes heat loss on the burner. This is expected as the flame is not adiabatic, figure (4.3b) show the enthalpy comparison, where heat loss can be observed which leads to enthalpy loss before 0.5mm. The temperature is also compared against detailed result which is shown in figure (4.3d), from these it can be concluded that two dimensional FGM method compares well detailed results from CHEM1D.

Two-dimensional contour plots are plotted to show the effects of an applied potential on flame characteristics, two cases of two-dimensional FGM results are taken with an applied potential of 0V and 100V. Figure (4.4) show for both applied potential, progress variable mass fraction and source term, and enthalpy remains the same and not effected by an applied electric field. This is same as observed from one-dimensional results where only charged species are effected by an applied potential.

Contour plots for the charged species mass fraction is shown in figure (4.5) for an applied potential of 20V and 100V. Figures (4.5a) and (4.5b) show the electrons move towards electrode with increase in potential from 20V to 100V, also the concentration of electrons are decreased. However, H_3O^+ move towards the burner side with increasing potential in figures (4.5c) and (4.5d), this is due to the electric field, charge separation occurs.

Figures (4.6a) and (4.6b) show the mass fraction distribution of electrons and H_3O^+ respectively. There are three cases considered in this figure, without applied potential, with an applied potential

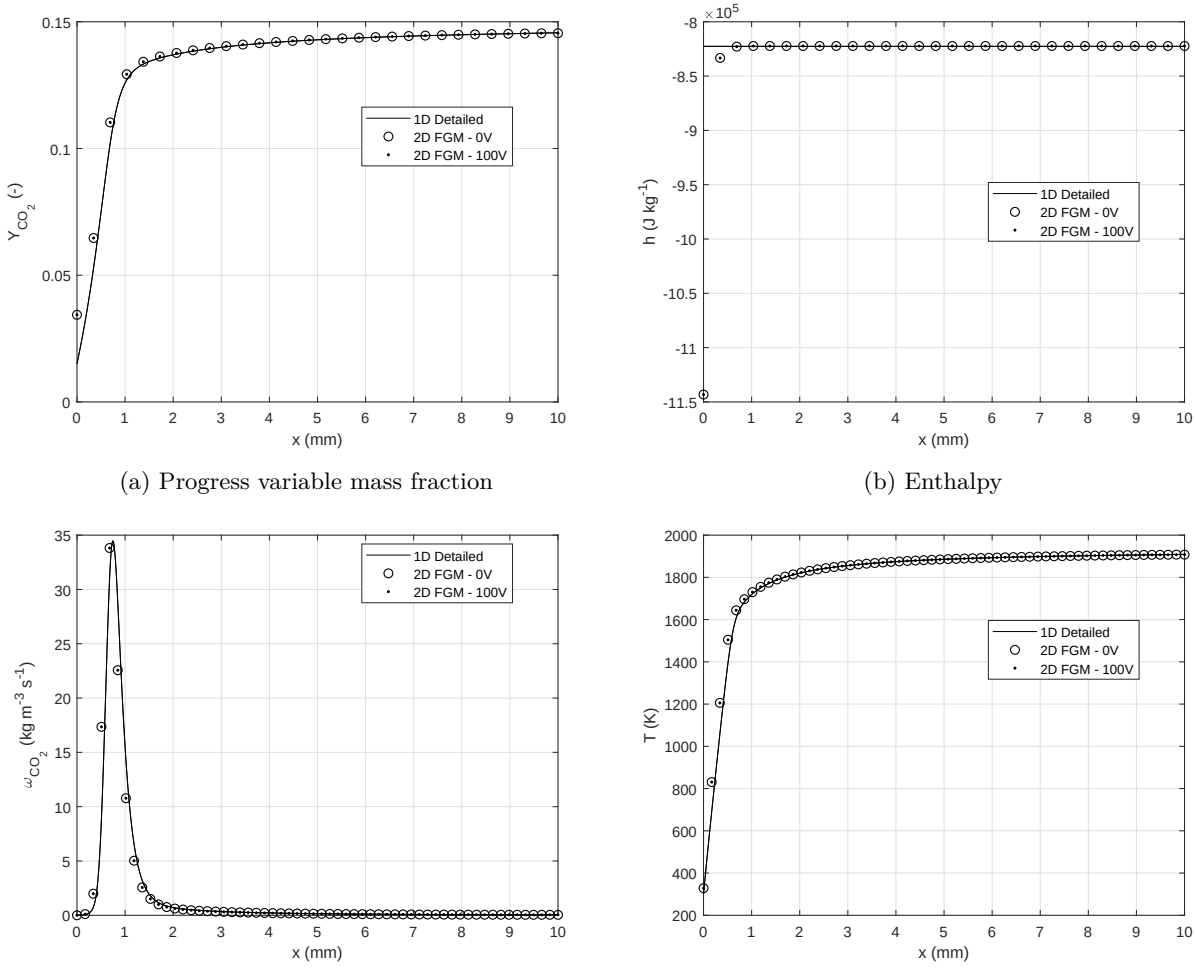

(a) Progress variable mass fraction

(b) Enthalpy

(c) Source progress variable

(d) Temperature

Figure 4.3: Comparison of two dimentional FGM results against detailed chemistry in one-dimensional.

of 20V and finally with an applied potential of 100V. It can be observed that for all potential, mass fraction of charged species from FGM result compares well with the 1D detailed result. For no applied potential case both charged species mass fraction peak is situated at 0.72mm from the burner. This is observed as small electric field keeps charged species together.

Now considering the non-saturation case of 20V, both charged species mass fraction peaks are approximately the same while the peaks are smaller than the case without applied potential. The electrons are absent near the burner while H_3O^+ is present at this region, and this charge separation is correctly calculated by the FGM method. As the electric field increases, electrons move towards the electrode while the burner attracts H_3O^+.

When the potential is increased to 100V which is saturated electric field in this case, the concentration of electron mass fraction nears to zero while H_3O^+ concentration drastically reduces at the burner side. As the electric field strength increases all the positive and negative ions move towards opposite polarities. Due to this effect the electron concentration is very low and this is well captured by FGM method.

(a) Progress variable mass fraction at 0V

(b) Progress variable mass fraction at 100V

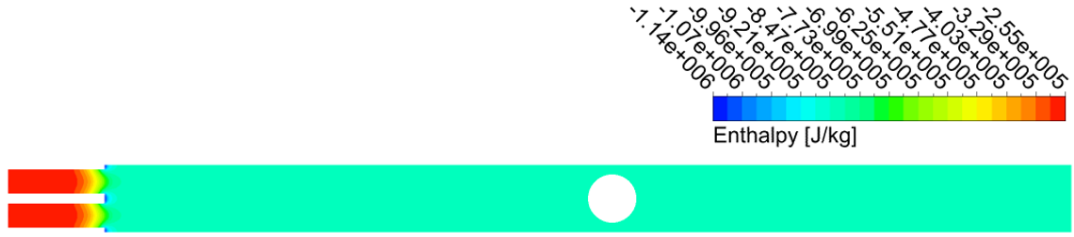

(c) Enthalpy at 0V

(d) Enthalpy at 100V

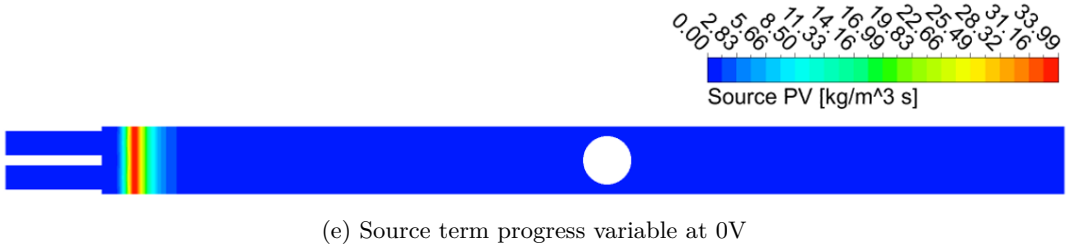

(e) Source term progress variable at 0V

(f) Source term progress variable at 100V

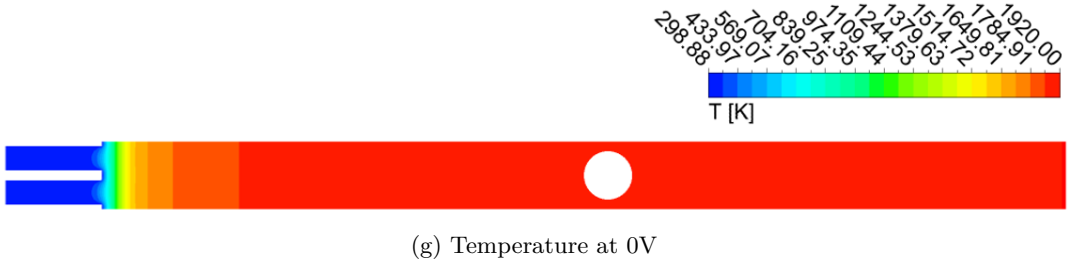

(g) Temperature at 0V

(h) Temperature at 100V

Figure 4.4: Comparison of two-dimentional FGM results with an applied potential of 0V and 100V.

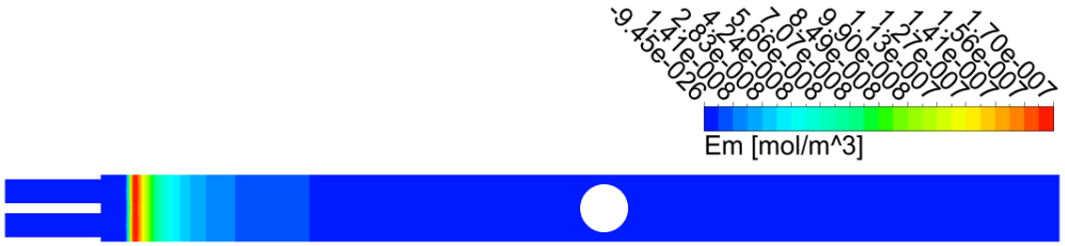

(a) Electron mass fraction at 20V

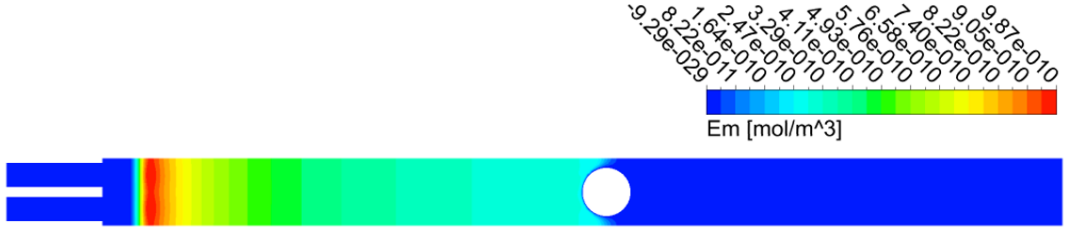

(b) Electron mass fraction at 100V

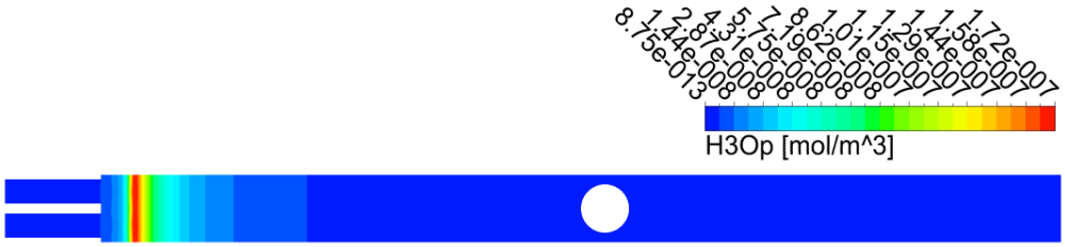

(c) H_3O^+ mass fraction at 20V

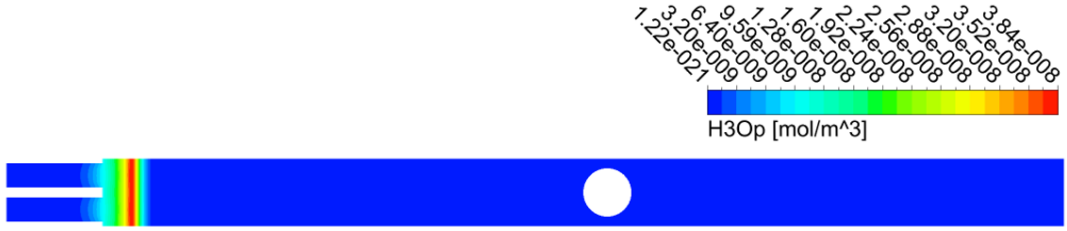

(d) H_3O^+ mass fraction at 100V

(e) Potential distribution of 20V

(f) Potential distribution of 100V

Figure 4.5: Comparison of two-dimentional FGM results for charged species mass fraction and potential for an applied potential of 20V and 100V.

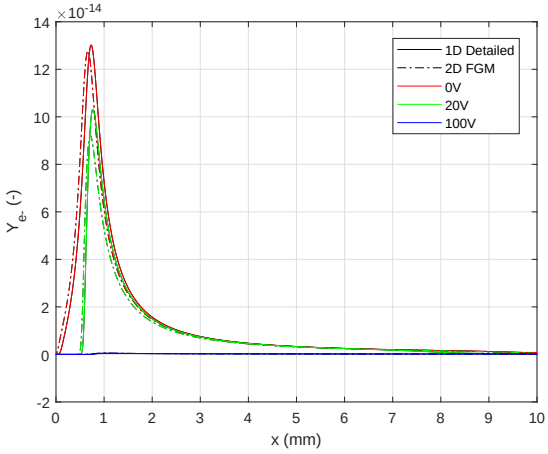

(a) Electron mass fraction

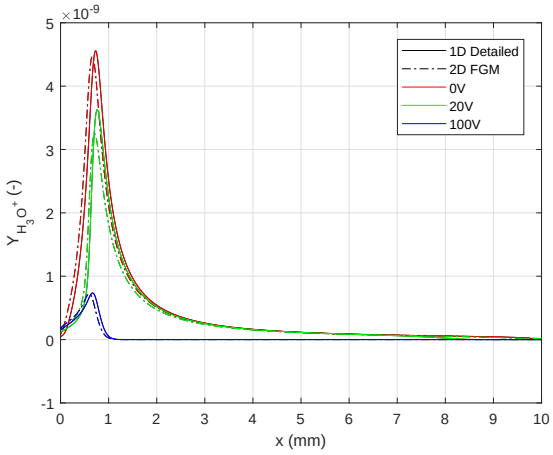

(b) H_3O^+ mass fraction

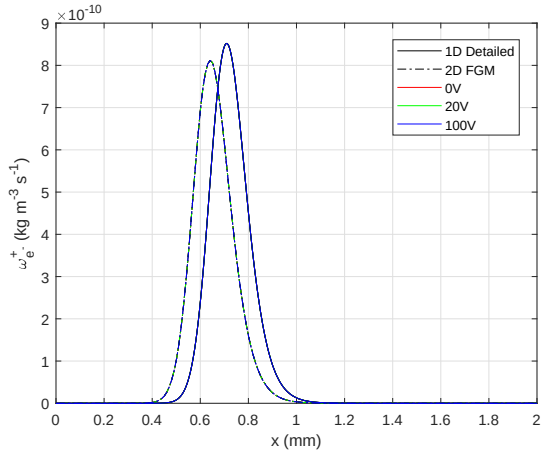

(c) Production of electron

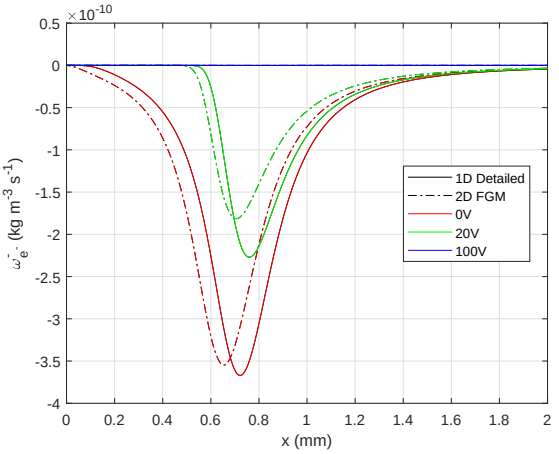

(d) Consumption of electron

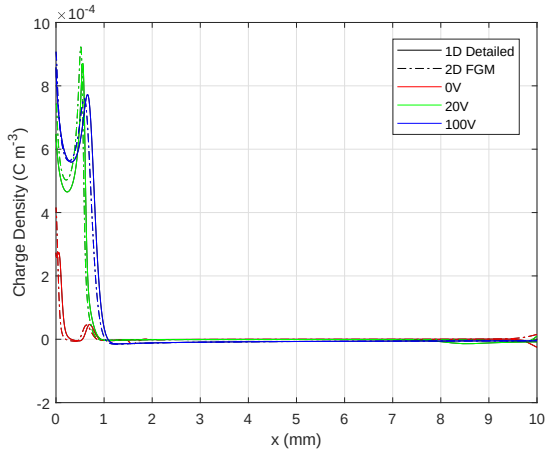

(e) Charge density

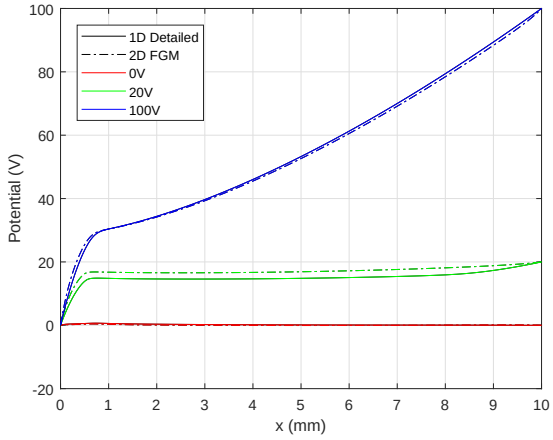

(f) Potential

Figure 4.6: Comparison of charged species mass fraction, production, consumption, charge density and potential for applied potential of 0V, 20V and 100V. Electrode distance is 10mm from the burner for production and consumption x-axis is limted to 2mm. Dash dotted line and solid line represents FGM and Detailed 1D results respectively.

Production and consumption of charged species for various applied potential are shown in figures (4.6c) and (4.6d). The production of charged species electrons are same for all applied potential. This is because the production of charged species are not affected by an applied electric field. But the consumption of charged species decreases with increasing electric field strength, as it has very little time to react with each other for recombination reaction. For an applied potential of 100V the consumption of charged species becomes near zero leading to no recombination reaction.

In figure (4.6f) for non-saturation 1D detailed condition of 20V, it can be observed that the potential has a steep curve 9mm from the burner. This is due to the boundary condition taken in 1D detailed, electrons are not present at this region and H_3O^+ are moved towards the burner leading to a negative charge density, which can be observed in figure (4.6e). For non-saturation conditions FGM potential distribution is higher than the 1D result. This is due to high charge density in the domain as shown. For higher potential, FGM matches well with the 1D detailed results, as can be observed from potential distribution for 100V, this might be caused by the strong electric force separation of all the charged species.

4.2.1 Electric current

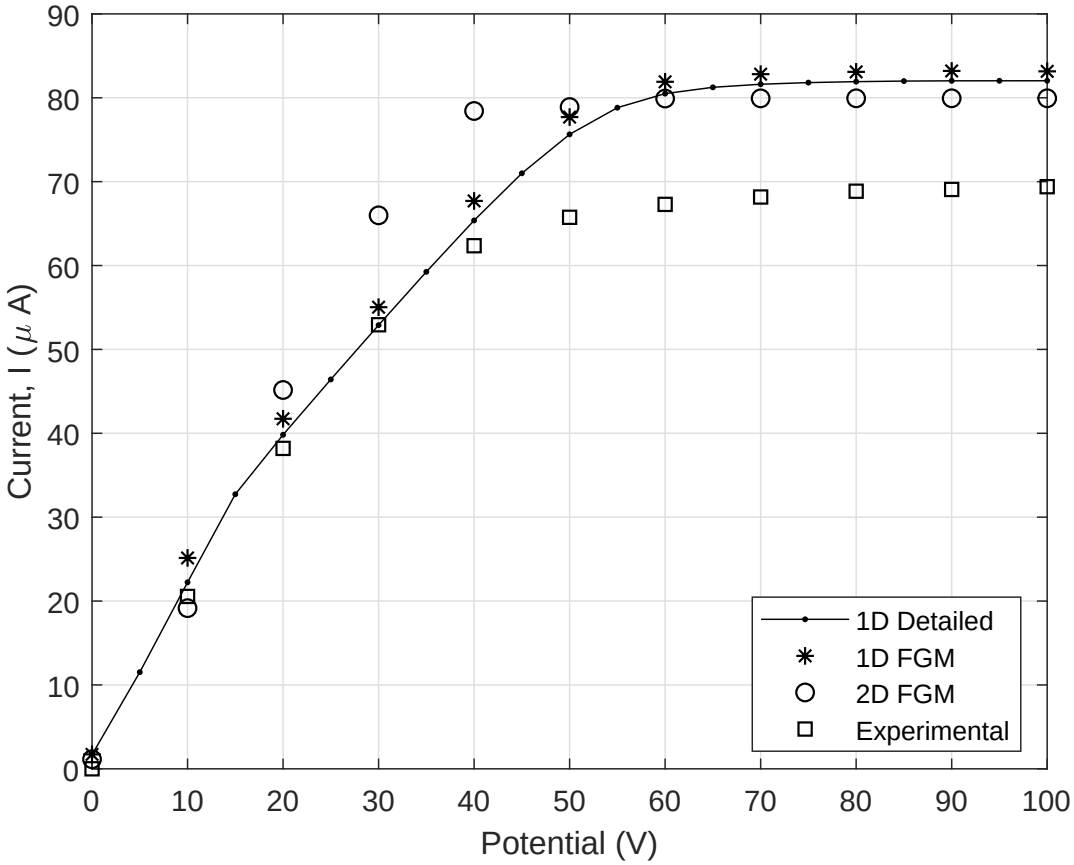

Figure 4.7: Comparison of simulated electric current in one-dimension and two-dimension with experimental values for an electrode distance of 10mm and equivalence ratio of 1.0

Simulated FGM electric current is validated against the experimental value, one-dimensional de-

tailed and FGM results. Figure (4.7) show the electric current plotted against an applied potential from 0V to 100V for an equivalence ratio of 1. The current is computed for an electrode distance of 10mm from the burner and the burner plate is considered to be the ground electrode. FGM method in two-dimensional domain calculates higher current in the non-saturation region, than the one-dimensional detailed and FGM result. Higher current is due to the higher consumption rate of charged species, figure (4.6d) show the higher consumption for 20V. Current is computed as the volume integral of charged species source term, as the two-dimensional domain has higher source term than the one-dimensional detailed, current is higher. The two-dimensional FGM current plot upto 40V has parabolic form whereas one-dimensional FGM has linear increase in current, similar to detailed result. So, The higher current in FGM might also be due to the effects of two-dimensional domain.

From figure it can be noticed that the saturation current for 1D detailed result, for an electrode distance of 10mm reaches at 70V, while for FGM this reaches at 50V. Comparing the FGM with the experimental results it can be observed that both have the same profile whereas 1D detailed has a steep increase from 15V while FGM has a smooth increase in current as potential increases. This is due to the two-dimensional effects where charge density is distributed in two-dimensional profile whereas in one-dimension it is constrained due to boundary condition.

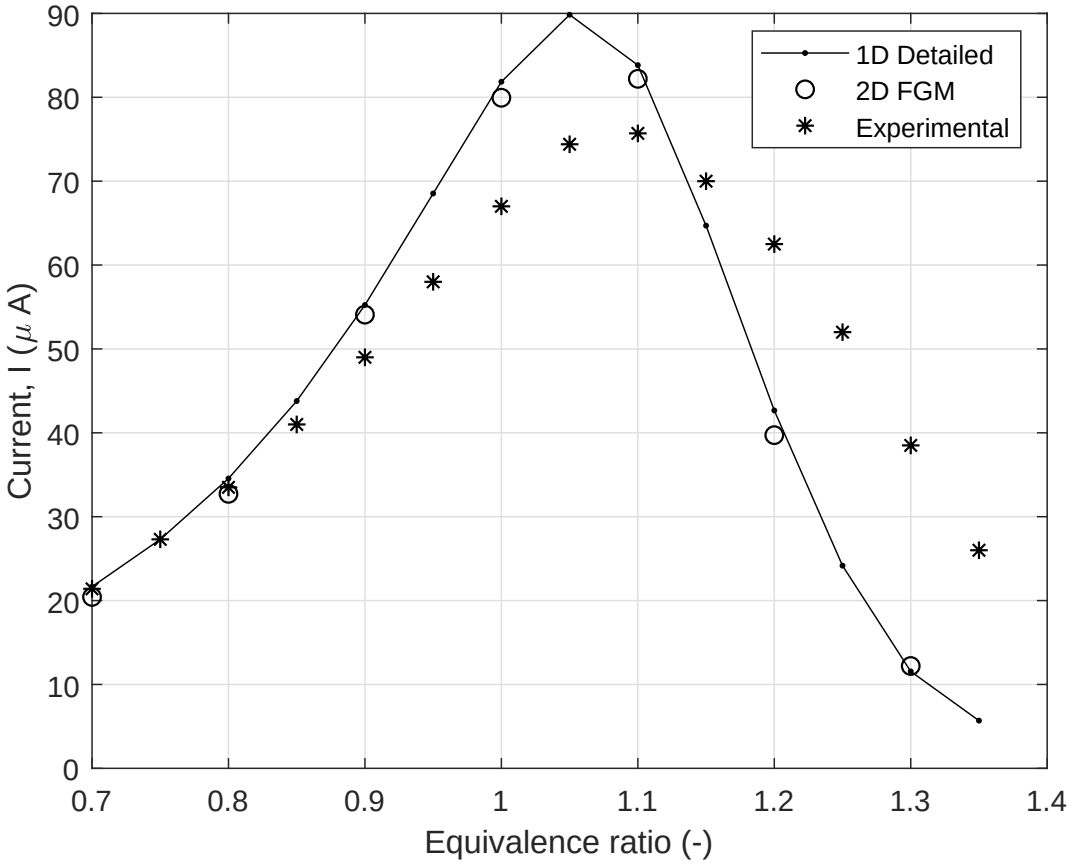

Figure 4.8: Comparison of simulated electric current with experimental values for an electrode distance of 10mm for equivalence ratio ranging from 0.7 to 1.35 at an applied potential of 300V.

As current is a function of charged species and the production of charged species is dependent on the equivalence ratio, it is important to study this relation. As an application example, in heat

boilers the equivalence ratio of the flame changes. To predict the current for different equivalence ratio a saturation case at 300V is considered and the equivalence ratio is varied from 0.7 to 1.35 with a step of 0.05 for experimental and 1D detailed while for FGM it is varied with 0.1.

FGM comapres well with the 1D detailed results for all equivalence ratios. For lean flame simulated current predicts well with the experimental results, while for rich flame above equivalence ratio of 1.1 experimental values does not match with the simulated results. This is expected as is it found by Jones [16], that there is an additional chemi-ionization reaction in rich flames. This leads to production of $C_3H_3^+$ and other additional charged species, which is not considered in this study. Simulated current also captures the peak values at equivalence ratio of 1.05 quite accurately. It can be concluded that the simulated current by the FGM method, matches well with the detailed chemistry and experimental results for lean flames.

4.2.2 Diodic effect

One of the important characteristics to check with FGM simulations is the diodic effect. This is the difference between slopes of the negative part of the voltage-current characteristic [27]. Due to high computational time entire current characteristics is not studied. Instead a comparison between a positive and negative potential of 300V is considered and studied. Figure (4.9) show mass fraction, source term of charged species, charge density and potential at an applied potential of -300V and 300V. FGM predicts well for both negative and positive potential when compared to 1D detailed results.

Considering the figures (4.9a) and (4.9b) it can be observed that the mass fractions of electron and H_3O^+ does not behave the same for different potentials. This effect is also shown in charged species electrons production and consumption in figures (4.9c) and (4.9d), where for +300V the consumption of electrons nears zero while consumption of -300V is high. Consumption of charged species at -300V is similar to an applied potential of 0V shown in figure (4.6). This is caused by to a low potential at reaction zone in the flame as observed from figure (4.9f). This is caused as H_3O^+ is heavier than the electrons, the electric field is not strong enough to dominate over Fickian diffusion, but it can be observed that the electrons are not present near the electrode and moved towards the burner at this electric field. As the distance between the negatively charged electrode and the flame front, is larger for the negative polarity and this causes the diodic effect [27].

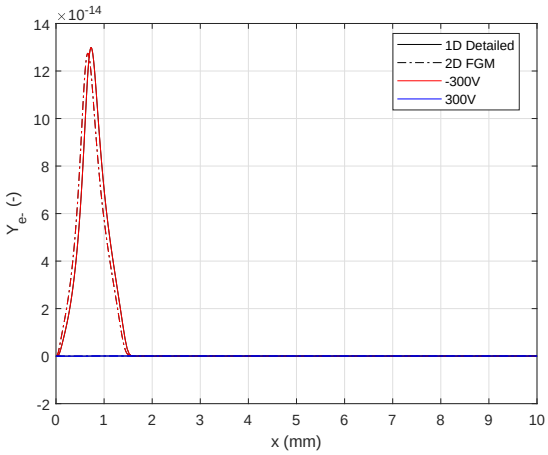

(a) Electron mass fraction

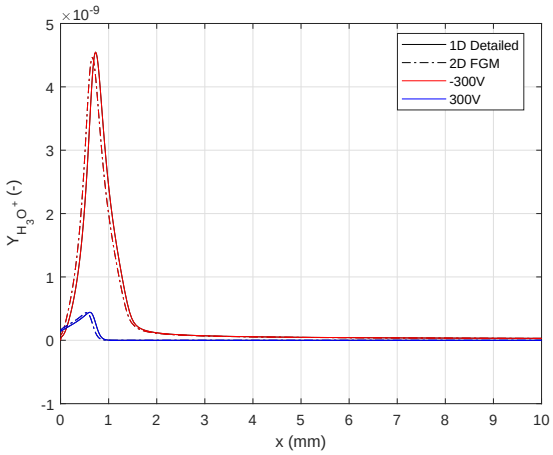

(b) H_3O^+ mass fraction

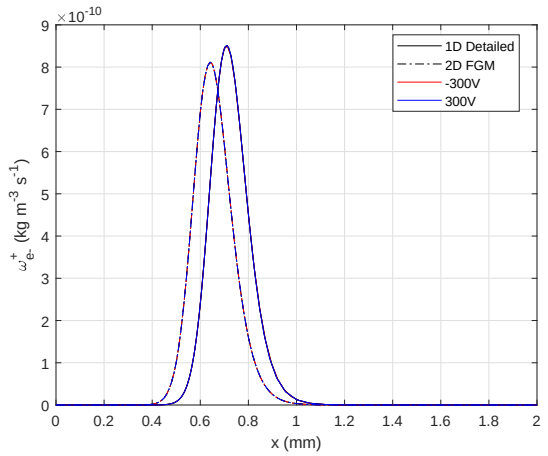

(c) Production and consumption of electron

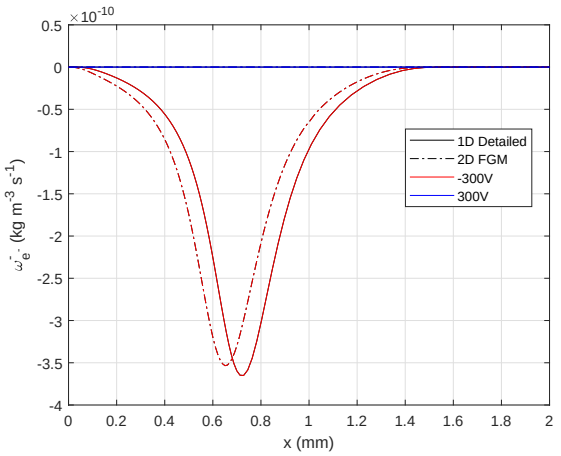

(d) Production and consumption of H_3O^+

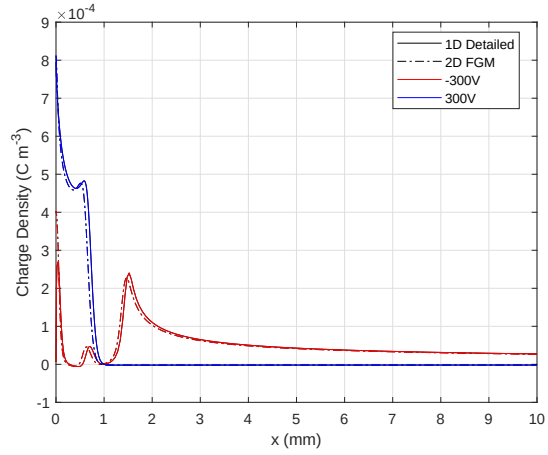

(e) Charge density

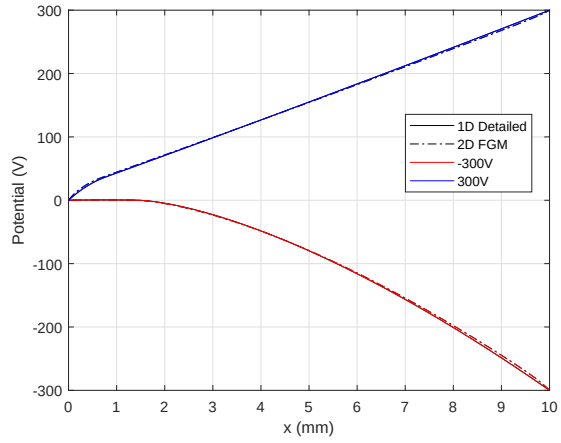

(f) Potential

Figure 4.9: Comparison of charged species mass fraction, production, consumption, charge density and potential for applied potential of -300V and 300V. Electrode distance is 10mm from the burner for production and consumption x-axis is limited to 2mm. Dash dotted line and solid line represents FGM and Detailed 1D results respectively.

4.3 Heat loss at electrode

In reality the electrode is not adiabatic, to check how FGM method predicts the case with heat loss. Electrode is considered to have heat loss by keeping it at 400K. Massflow and inlet temperature are taken to be same, figure (4.10b) show the enthalpy plot compared with adiabatic result. At burner and at electrode enthalpy drop can be observed, this is caused when the flame comes in contact with the cooled surface which causes heat loss. Due to the rapid heat loss at the electrode the flame is slightly pushed back as can be seen from figure (4.10a). The heat loss effects can be clearly observed from two-dimensional contour plots shown in figures (4.12a) and (4.12b), where the effect of heat loss at the electrode leads enthalpy to decrease from -1.14MJ/kg to -2.87MJ/kg.

To check how charge species behaves under heat loss affects, a case with an applied potential of 20V is considered figure (4.11). It is already discussed that FGM predicts higher potential at 20V compared to detailed result, with heat loss it has even higher potential distribution when compared with adiabatic FGM case as shown in figure (4.11f). The reason for this is due to higher charge density near the electrode as can be seen in figure (4.11e). Higher charge density is looked up due to heat loss near the electrode which result in higher potential distribution.

Due to the higher potential distribution the consumption of charged species (H_3O^+ and e^-) is also higher from figures (4.11c) and (4.11d). However, the production of charged species are not effected, this is expected as the production of charged species is independent of potential. Due to the higher consumption the mass fraction of the charged species are also lower and the peak of the both charged species are much lower compared to adiabatic case from figures (4.11a) and (4.11b). From two-dimensional contour plots the charged species show the same movement for an applied potential for both adiabatic and heat loss cases figure (4.12), but the concentrations are much lower for the heat loss case compared to adiabatic due to the higher potential distribution.

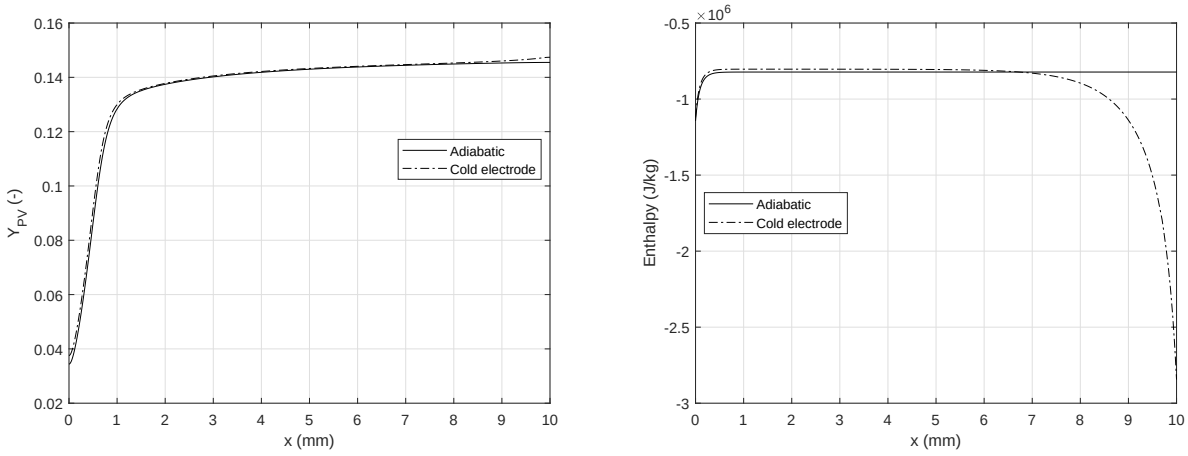

(a) Progress variable mass fraction

(b) Enthalpy

Figure 4.10: Comparison of two dimentional FGM results considering adiabatic and heat loss at electrode.

Electric current

Electric current computed from two-dimensional simulation for adiabatic cases where compared with detailed results. In this section the heat loss effects is considered at the electrode and

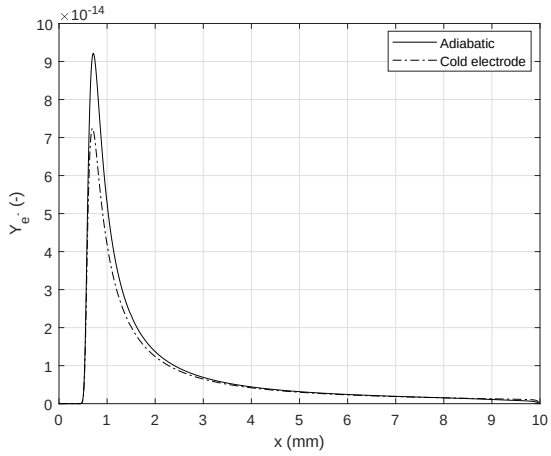

(a) Electron mass fraction

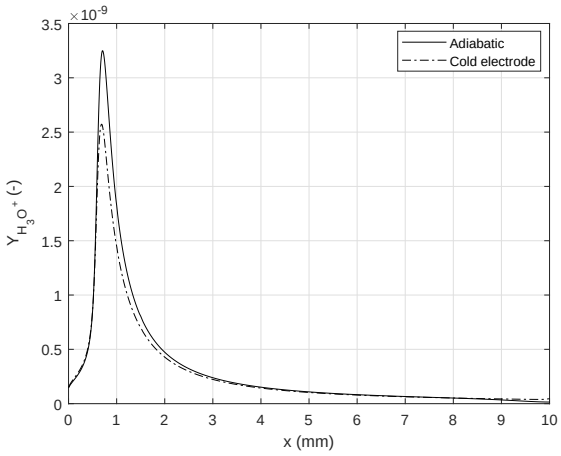

(b) H_3O^+ mass fraction

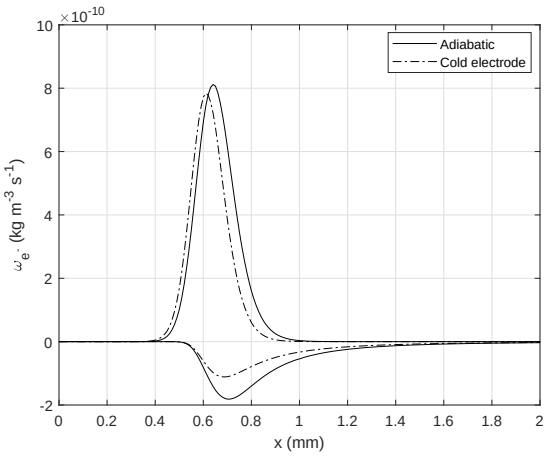

(c) Production and consumption of electron

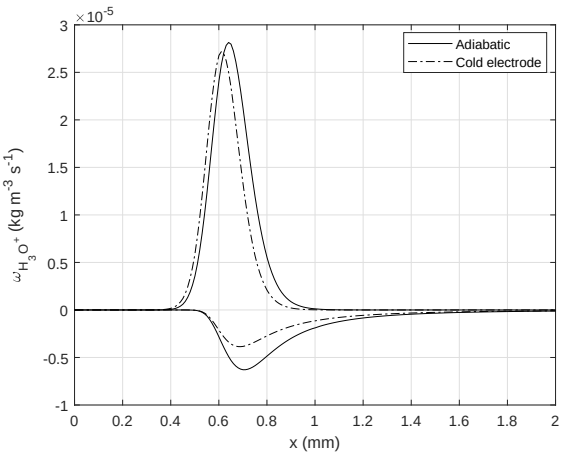

(d) Production and consumption of H_3O^+

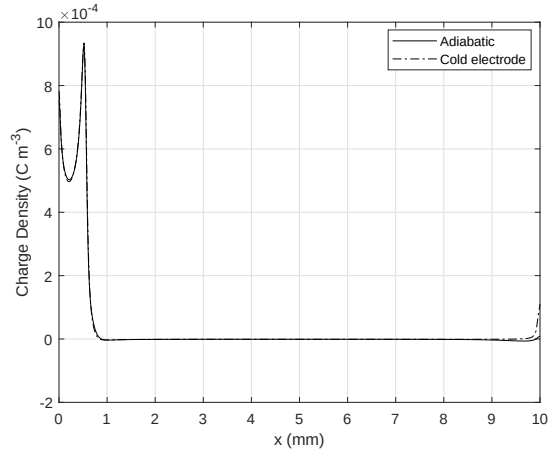

(e) Charge density

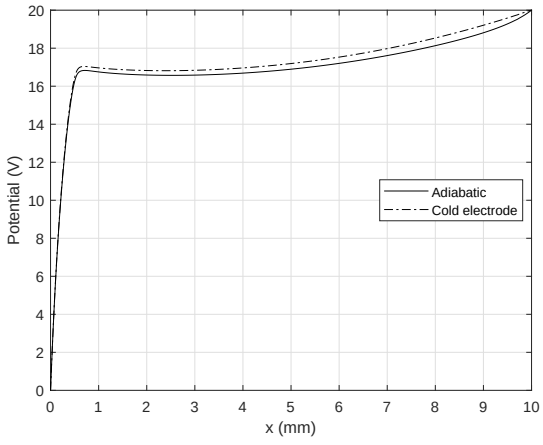

(f) Potential

Figure 4.11: Comparison of charged species mass fraction, production, consumption, charge density and potential for applied potential of 20V with heat loss at electrode and adiabatic case. Electrode distance is 10mm from the burner, dash dotted line and solid line represents FGM with heat loss and adiabatic cases respectively.

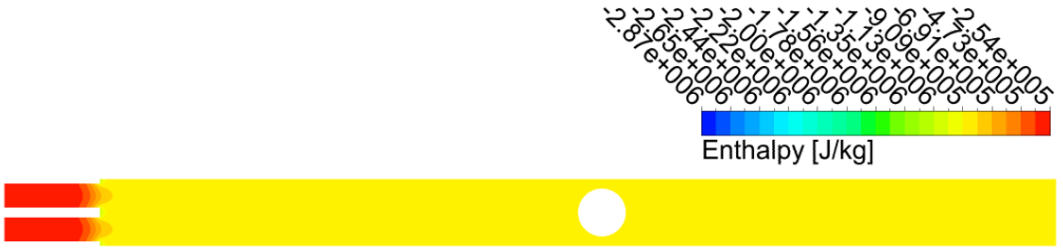

(a) Adiabatic enthalpy at 20V

(b) Heat loss enthalpy at 20V

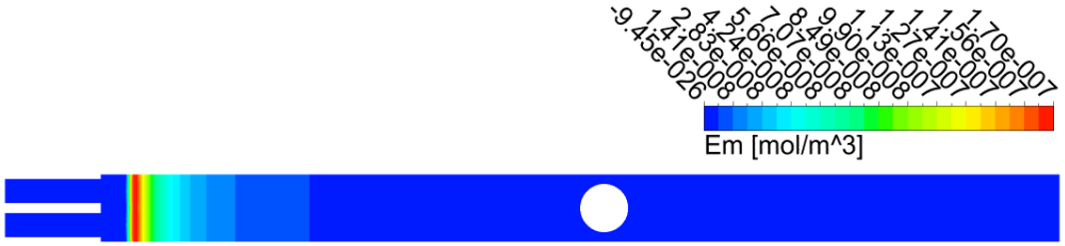

(c) Adiabatic e^- mass fraction at 20V

(d) Heat loss e^- mass fraction at 20V

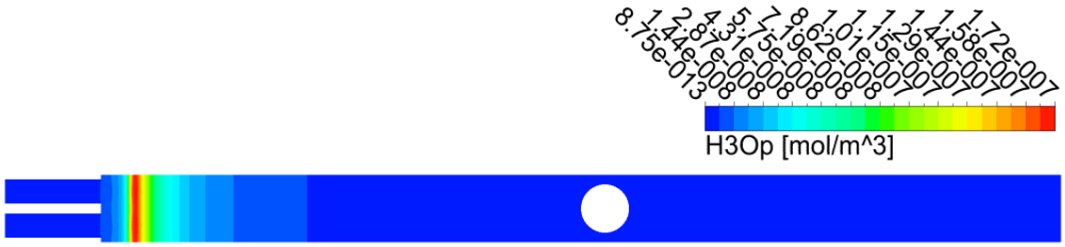

(e) Adiabatic H_3O^+ of 20V

(f) Heat loss H_3O^+ of 20V

Figure 4.12: Comparison of FGM results of adiabatic and heat loss case for an applied potential of 20V.

the electric current computed with heat loss effects are compared with adiabatic results and experimental values as shown in figure (4.13). The electric current due to heat loss effects computes higher current than adiabatic case upto 30V of potential, due to the higher potential distribution in the heat loss case. The heat loss case reaches saturation current at 40V itself, and the saturation current is same as the experimental result. The lower saturation current in heat loss case compared to adiabatic case is due to the lower charge species source term as observed in figure (4.11c).

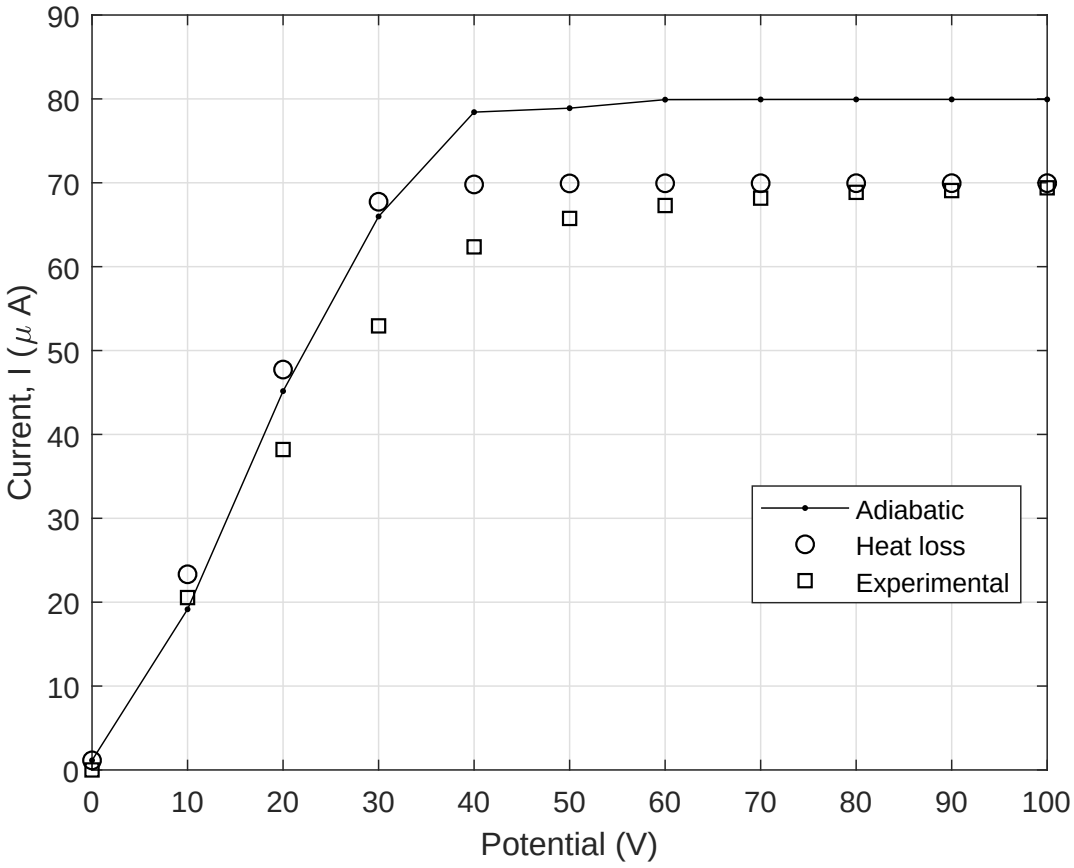

Figure 4.13: Comparison of simulated electric current of adiabatic and heat loss case with experimental values for an electrode distance of 10mm.

4.4 Conclusions

The FGM model studied in Chapter 3 is used to study ionization mechanism in two dimensional geometry. It is concluded that the FGM model matches well with the 1D detail with and without applied electric field. The FGM model is studied and compared with detailed model for various applied electric field, it is found that for saturation electric field FGM matches well with the detailed model whereas for non-saturation condition FGM model computes higher potential than the detailed. This is caused due to distribution of charged species in the domain for FGM method, while in 1D detailed due to boundary condition, on application of electric field charged species are absent near the boundary. This causes a steep decrease on potential for non-saturation condition.

The model is used to compare the simulated electric current with detailed model and experimental

values. This is compared for varying potential for an equivalence ratio of 1 and at saturation potential of 300V for varying equivalence ratio. It is concluded that the computed current is in-line with the detailed results for saturation condition whereas for lower potential it is higher than detailed results. This is caused due to the higher potential which is computed in FGM model.

The FGM model is also accurately computes the diodic effect which is caused due to difference in diffusivity between electron and H_3O^+. Due to negative electric field the distance which positive ion has to travel to reach electrode is large. Due to its higher mass than electron and lower diffusivity the electric field is not strong enough to over come the Fickian diffusion and to reach electrode. This difference in positive and negative applied potential is termed as diodic effect and FGM model computes this effect accurately when compared to detailed model.

Finally, the model is also used to compute the effects of the heat loss at the electrode, for an applied potential the lookup of the production of charged species is less in heat loss case when compared to adiabatic case. It is found that the potential distribution is higher in heat loss case compared to adiabatic case which results in higher current in non-saturation regime. However, due to the less production rate of charged species the saturation current is lesser than adiabatic current.

Chapter 5

Conclusions and recommendations

5.1 Conclusions

The aim of this study was to combine the ionization mechanism, considered in the study of Speelman, with the Flamelet generated manifold (FGM) method and compare the simulated results with the detailed and experimental values. The model uses flat ionized flames to simulate the electric current with applied electric fields. FGM uses lookup method to compute species by only solving desired number of transport equations (enthalpy and progress variable). This method can not be applied to lookup charged species, as the effect of an applied electric field on charged species are not captured. To overcome this problem, three additional transport equations are solved by FGM. Two for charged species (e^- and H_3O^+) and one for potential equation, by doing so charged species distribution can be captured on application of an applied electric field.

In Chapter 3 one-dimensional results of ionization mechanism are studied using the FGM method. To reduce the computational time constant Lewis diffusion model is implemented to ionization mechanism, and found that the constant Lewis model compares well with the multi-component diffusion model. The one-dimensional application of FGM ionization mechanism validates well with the detailed results, and also the current computed for different applied potential using FGM method compares well with the detailed results.

The FGM method with ionization mechanism is extended to two-dimensional model to see the effect of an applied potential on charged species. Considering the electrode as adiabatic, for saturation potential a good comparison is observed when compared with detailed results, while for non-saturation potential a higher potential distribution in FGM is observed which is caused due to high charge density in the domain. Now, considering heat loss at the electrode, it is found that for non-saturation case the potential distribution is higher than the FGM case. This is caused due to the higher H_3O^+ distribution in the domain which leads to higher charge density leading to higher potential, intern leading to higher consumption for charged species. It is observed that due to the heat loss effects it is seen that the flame is slightly pushed back.

Electric current computed from the two-dimensional FGM results are compared with both one-dimensional detailed results and experimental values, for varying potential and equivalence ratio. Electric current computed from FGM saturates at lower potential than detailed and experimental values in both adiabatic and heat loss cases. Saturation electric current due to heat loss matches well with the experimental value, whereas in adiabatic case higher current is computed. This is

due to lower production rate of charged species in the heat loss case compared to slightly higher production rate in adiabatic case.

It can be concluded that electric flux is currently implemented in Ansys Fluent for computing the effects of charged species on application of an applied potential using FGM method. This will reduce the computing time for the calculation of the ionization mechanism on an applied electric field. FGM method also predicts accurately the diodic effect and matches well with the detailed results.

5.2 Recommendations

The FGM method modeled for the ionization phenomenon is studied for one-dimensional and two-dimensional domains. Comparing one-dimensional and two-dimensional simulation results for an applied potential, the potential distribution in two-dimensional domain is higher than one-dimensional domain. To get the realistic charge distribution, and to check the accuracy of the model for predicting the electric current, it is good to further study the model using three-dimensional domain. As this results in a realistic flame structure, the accuracy of the FGM method can be further studied for predicting the electric current.

This study only focus on only two charged species (e^- and H_3O^+), which result in good approximation for detecting the electric current for lean methane-air fuel. For fuel-air ratio above 1.1, the prediction of electric current is not accurate. This is due to the change in chemi-ionization reaction, as the fuel-air ratio changes from lean to rich mixture fuels. In rich mixture fuels there is an additional chemi-ionization reaction which leads to $C_3H_3^+$ ion. To get a better accuracy for all the equivalence ratio, a more realistic ionization mechanism should be modeled, with the inclusion of other abundant charged species. This might give a better accuracy for predicting the electric current for all equivalence ratio from lean to rich.

Furthermore, the only fuel studied in this case is methane-air fuel. To check the accuracy of the ionization model, different fuels must be considered and studied for example C_3H_8 or H_2. By studying the ionization model for different fuels, the accuracy of the model can be observed. This gives an insight whether, the ionization mechanism changes if the fuels is different or is it the same. Also how accurately the FGM model can predict the ionization model for different fuels.

For an applied potential of 0V the FGM method in two-dimensional domain is computationally intensive, this might be reduced by improving the numerical stability of the code. Due to the internal electric field created by the charged species, both charged species should stay close together. In steady case simulation, the convergence of this simulation at 0V is computationally expensive. So, the stability of the code should be improved. One of the way it can be checked, by changing the boundary conditions for the electric flux at burner and electrode side.

References

[1] J.D. Anderson. Fundamentals of Aerodynamics. *McGraw-Hill series in aeronautical and aerospace engineering series.*, 2001.

[2] M. Belhi, P. Domingo, and P. Vervisch. Effect of electric field on flame stability. *Proceedings of the European Combustion Meeting*, 0:1–6, 2009. URL `http://combustion.org.uk/ECM{_}2009/P810320.pdf`.

[3] M. Belhi, P. Domingo, and P. Vervisch. Direct numerical simulation of the effect of an electric field on flame stability. *Combustion and Flame*, 157(12):2286–2297, 2010. ISSN 00102180. doi: 10.1016/j.combustflame.2010.07.007. URL `http://dx.doi.org/10.1016/j.combustflame.2010.07.007`.

[4] G. Blanquart, P. Pepiot-Desjardins, and H. Pitsch. Chemical mechanism for high temperature combustion of engine relevant fuels with emphasis on soot precursors. *Combustion and Flame*, 156(3):588–607, 2009. ISSN 00102180. doi: 10.1016/j.combustflame.2008.12.007. URL `http://dx.doi.org/10.1016/j.combustflame.2008.12.007`.

[5] K. J. Bosschaart and L. P. H. de Goey. Detailed analysis of the heat flux method for measuring burning velocities. 132(1-2):170–180, 2003. doi: 10.6100/IR560010.

[6] L.P.H. de Goey, A. van Maaren, and R.M. Quax. Stabilization of Adiabatic Premixed Laminar Flames on a Flat Flame Burner. *Combustion Science and Technology*, 92(November 2015): 201–207, 1993. ISSN 0010-2202. doi: 10.1080/00102209308907668.

[7] H. Duan, X. Wu, T. Sun, B. Liu, J. Fang, C. Li, and Z. Gao. Effects of electric field intensity and distribution on flame propagation speed of CH4/O2/N2 flames. *Fuel*, 158:807–815, 2015. ISSN 00162361. doi: 10.1016/j.fuel.2015.05.065. URL `http://linkinghub.elsevier.com/retrieve/pii/S0016236115005724`.

[8] H. Duan, X. Wu, J. Hou, C. Zhang, and Z. Gao. Experimental study of lean premixed CH4/N2/O2 flames under low-frequency alternating-current electric fields. *Fuel*, 181:1011–1019, 2016. ISSN 00162361. doi: 10.1016/j.fuel.2016.05.008. URL `http://dx.doi.org/10.1016/j.fuel.2016.05.008`.

[9] Y. Gan, M. Wang, Y. Luo, X. Chen, and J. Xu. Effects of direct-current electric fields on flame shape and combustion characteristics of ethanol in small scale. *Advances in Mechanical Engineering*, 8(1):1–14, 2016. ISSN 1687-8140. doi: 10.1177/1687814015624846. URL `http://ade.sagepub.com/lookup/doi/10.1177/1687814015624846`.

[10] J M Goodings, D K Bohme, and C W Ng. Detailed ion chemistry in methane oxygen flames. I. Positive ions. *Combustion and Flame*, 36:27, 1979.

[11] J. M. Goodings, D. K. Bohme, and C. W. Ng. Detailed ion chemistry in methane oxygen flames. I. Positive ions. *Combustion and Flame*, 36:27, 1979.

[12] J. A. Green and T. M. Sugden. Some observations on the mechanism of ionization in flames containing hydrocarbons. *Symposium (International) on Combustion*, 9(1):607–621, 1963. ISSN 00820784. doi: 10.1016/S0082-0784(63)80070-3.

[13] C. Guerra-Garcia and M. Martinez-Sanchez. Counterflow nonpremixed flame DC displacement under AC electric field. *Combustion and Flame*, 162(11):4254–4263, 2015. ISSN 00102180. doi: 10.1016/j.combustflame.2015.07.038. URL http://www.sciencedirect.com/science/article/pii/S0010218015002461{%}5Cnhttp://linkinghub.elsevier.com/retrieve/pii/S0010218015002461.

[14] J. Han, M. Belhi, T. A. Casey, F. Bisetti, H. G. Im, and J. Y. Chen. The i-V curve characteristics of burner-stabilized premixed flames: Detailed and reduced models. *Proceedings of the Combustion Institute*, 36(1):1241–1250, 2015. ISSN 15407489. doi: 10.1016/j.proci.2016.05.056. URL http://dx.doi.org/10.1016/j.proci.2016.05.056.

[15] A. N. Hayhurst, J. M. Goodings, and S. G. Taylor. The effects of applying electric fields on the mass spectrometric sampling of positive and negative ions from a flame at atmospheric pressure. *Combustion and Flame*, 161(12):3249–3262, 2014. ISSN 15562921. doi: 10.1016/j.combustflame.2014.06.012. URL http://dx.doi.org/10.1016/j.combustflame.2014.06.012.

[16] H. R. N. Jones and A. N. Hayhurst. Measurements of the concentrations of positive and negative ions along premixed fuel-rich flames of methane and oxygen. *Combustion and Flame*, 166:86–97, 2016. ISSN 00102180. doi: 10.1016/j.combustflame.2016.01.003. URL http://dx.doi.org/10.1016/j.combustflame.2016.01.003.

[17] B.J.P. Joris. Development of the FGM method on predicting CO emissions for laminar premixed cooled lean methane/air flames. *Master Thesis.*, August 2012.

[18] J. Kuhl, T. Seeger, L. Zigan, S. Will, and A. Leipertz. On the effect of ionic wind on structure and temperature of laminar premixed flames influenced by electric fields. *Combustion and Flame*, 176:391–399, 2017. ISSN 0010-2180. doi: 10.1016/j.combustflame.2016.10.026. URL http://dx.doi.org/10.1016/j.combustflame.2016.10.026.

[19] W. J. Liang and T. H. Lin. The Characteristics of Ionic Wind and Its Effect on Electrostatic Precipitators. *Aerosol Science and Technology*, 20(4):330–344, 1994. ISSN 0278-6826. doi: 10.1080/02786829408959689. URL http://www.tandfonline.com/doi/abs/10.1080/02786829408959689.

[20] W. J. Miller. Ions in flames. Evaluation and prognosis. *Symposium (International) on Combustion*, 14(1):307–320, 1973. ISSN 00820784. doi: 10.1016/S0082-0784(73)80031-1.

[21] J.A. van Oijen and L.P.H. de Goey. Modelling of Premixed Laminar Flames using Flamelet-Generated Manifolds. *Combustion Science and Technology*, 161(1):113–137, 2000. ISSN 0010-2202. doi: 10.1080/00102200008935814. URL http://www.tandfonline.com/doi/abs/10.1080/00102200008935814.

[22] L. B. W. Peerlings, Manohar, V. N. Kornilov, and L. H. P. de Goey. Flame ion generation rate as a measure of the flame thermo-acoustic response. *Combustion and Flame*, 160(11):2490–2496, 2013. ISSN 00102180. doi: 10.1016/j.combustflame.2013.05.014. URL http://dx.doi.org/10.1016/j.combustflame.2013.05.014.

[23] J. Prager, U. Riedel, and J. Warnatz. Modeling ion chemistry and charged species diffusion in lean methane-oxygen flames. *Proceedings of the Combustion Institute*, 31 I:1129–1137, 2007. ISSN 15407489. doi: 10.1016/j.proci.2006.07.141.

[24] Smith, G. P., D. M. Golden, M. Frenklach, N. W. Moriarty, B. Eiteneer, M. Goldenberg, C. T. Bowman, S. Song R. K. Hanson, I. V. Lissianski W. C. Gardiner, Jr., and Z. Qin. GRI-Mech 3.0. URL http://www.me.berkeley.edu/gri{_}mech/.

[25] L.M.T. Somers. The simulation of flat flames with detailed and reduced chemical models. *Ph. D. Dissertation.*, (September), 1994. doi: 10.6100/IR420430. URL `http://alexandria.tue.nl/repository/books/420430.pdf`.

[26] L.M.T. Somers. Governing equations. *In J.A. van Oijen, editor, J.M. Burgerscentrum Course on Combustion, J.M. Burgerscentrum Courses*, pages 13–31, Sep 2010.

[27] N. Speelman. Model development for ionization phenomena in premixed laminar flames. *Ph. D. Dissertation.*, 2015.

[28] N. Speelman, L.P.H. de Goey, and J.A. van Oijen. Development of a numerical model for the electric current in burner-stabilised mathane/air flames. *Combustion Theory and Modelling*, 19(2):159–187, 2015. ISSN 1364-7830. doi: 10.1080/13647830.2014.998712. URL `http://www.tandfonline.com/doi/abs/10.1080/13647830.2014.998712`.

[29] N. Speelman, M. Kiefer, D. Markus, U. Maas, L. P H de Goey, and J. A. van Oijenv. Validation of a novel numerical model for the electric currents in burner-stabilized methane-air flames. *Proceedings of the Combustion Institute*, 35(1):847–854, 2015. ISSN 15407489. doi: 10.1016/j.proci.2014.05.067. URL `http://dx.doi.org/10.1016/j.proci.2014.05.067`.

[30] E. N. Volkov, V. N. Kornilov, and L. P. H. de Goey. Experimental evaluation of DC electric field effect on the thermoacoustic behaviour of flat premixed flames. *Proceedings of the Combustion Institute*, 34(1):955–962, 2013. ISSN 15407489. doi: 10.1016/j.proci.2012.06.175. URL `http://dx.doi.org/10.1016/j.proci.2012.06.175`.

[31] F.M. White. Viscous Fluid Flow. *McGraw-Hill series in aeronautical and aerospace engineering series.*, pages 13–31, April 2005.

[32] F. A. Williams. Turbulent Combustion. pages 97–131, 1985.

[33] G. Wortberg. Ion-concentration measurements in a flat flame at atmospheric pressure. *Symposium (International) on Combustion*, 10(1):651–655, 1965. ISSN 00820784. doi: 10.1016/S0082-0784(65)80210-7.

[34] Y. Xiong, D. G. Park, B. J. Lee, S. H. Chung, and M. S. Cha. DC field response of one-dimensional flames using an ionized layer model. *Combustion and Flame*, 163:317–325, 2016. ISSN 15562921. doi: 10.1016/j.combustflame.2015.10.007. URL `http://dx.doi.org/10.1016/j.combustflame.2015.10.007`.

TU/e Technische Universiteit Eindhoven University of Technology

Declaration concerning the TU/e Code of Scientific Conduct for the Master's thesis

I have read the TU/e Code of Scientific Conduct[i].

I hereby declare that my Master's thesis has been carried out in accordance with the rules of the TU/e Code of Scientific Conduct

Date

25-01-2018

Name

A. KEELARA CHANDRASHEKAR

ID-number

0979634

Signature

Submit the signed declaration to the student administration of your department.

[i] See: http://www.tue.nl/en/university/about-the-university/integrity/scientific-integrity/
The Netherlands Code of Conduct for Academic Practice of the VSNU can be found here also.
More information about scientific integrity is published on the websites of TU/e and VSNU